University of Tartu

Faculty of Science and Technology

Institute of Chemistry

Roland Hoxha

SPECTROSCOPIC ELLIPSOMETRY AS A VERSATILE TOOL TO STUDY THIN FILMS GROWN BY ATOMIC LAYER DEPOSITION

Master's Thesis (30 ECTS)

Supervisors: Dr. Kaupo Kukli

Dr. Aile Tamm

Tartu, 2014

Contents

Abbreviations

ALD	Atomic Layer Deposition
VLSI	Very Large Scale Integrated
ALE	Atomic Layer Epitaxy
SE	Spectroscopic Ellipsometry
RCE	Rotating Compensator Ellipsomentry
SEM	Scanning Electron Microscopy
HRTEM	High Resolution Transmission Electron Microscopy
XRR	X-Ray Reflectivity
UV-VIS	Ultra Violet-Visible
PSA	Polarization State Analyzer
GRC	Growth Rate per Cycle
RAE	Rotating Analyzer Ellipsometry
RCE	Rotating Compensator Ellipsometry
PME	Phase-Modulation Ellipsometry
VASE	Variable Angle Spectroscopic Ellipsometry
PSG	Polarization State Generator

1. Introduction

1.1 Background of this study

In our daily life we are surrounded by electronic devices which have inside some or many microelectronic parts even though we do not see them. The working performance of electronic devices in general, and microelectronics especially, is closely related to the quality of their constituent components [1, 2].

Among the key components of modern microelectronic and photonic products are various types of thin film materials, which play an important role in their performance [1]. A thin film in our context is a layer of solid material ranging in thickness from fractions of a nanometer (monolayer) to several micrometers. A familiar example of thin film application is a simple mirror which is a sheet of glass coated on the backside with thin metal film, to form a reflective interface (fig. 1.a), or sunglasses which are designed primarily to protect our eyes against ultraviolet radiation (fig.1b). Electronic semiconductor devices (fig. 1c) and optical coatings are the main applications benefiting from thin-film construction [3].

Fig.1 Main applications of thin films in daily products. a) a household mirror, b) sunglasses, c) a very-large-scale integrated (VLSI) circuit.

In modern technology, in a variety of applications, including semiconductor microelectronics, displays, optical filters, magnetic information storage and catalysis, thin films have to meet the demands for specific device requirements [1, 3, 4].

On the manufacturing yield of integrated circuits, small variations in film uniformity can have a large influence. For very-large-scale integrated (VLSI) circuits (fig. 1c), at present, film

uniformity deviations, should not exceed 5%. Even more stringent the uniformity requirements are expected to become in the near future, decreasing to a deviation limit of 1 to 2%. [4]

In a device fabrication process sequence, thin films have to be deposited even on a non-planar surface and the film deposited should be uniform across all structural details of the substrate topography. For example, in VLSI circuit structures, contact holes with micron or submicron dimensions should be uniformly coated with metal films not only inside the small contact cavities, but also on their vertical walls [4]. This is referred to as step coverage or conformality.

Among the thin film deposition methods, the one which is particularly suitable for making uniform and conformal film layers is atomic layer deposition (ALD) also known as atomic layer epitaxy (ALE) [5].

Uniformity of thickness is an important requirement for thin solid films used in electronic and optoelectronic devices [6]. Uniform conformal films can be successfully grown by ALD. In addition, this thin film growth method allows for exact control of film thickness [5, 7].

1.2 Atomic Layer Deposition (ALD)

1.2.1 Introduction

With scaling down of semiconductor devices, due to its inherent benefits [8] compared to other thin film deposition techniques, the application of ALD has sparked a good deal of interest. Especially for nano-scale devices, in where each of the layers should be as thin and perfect as possible. Deposition of thin films with this method has become very important in recent years, particularly for growing the latest transistor gate oxides in modern integrated circuit chips [7].

1.2.2 Principle of ALD

An ALD process deposits thin layers of solid materials by using two or more different vapour-phase reactants.

In ALD, growth is controlled at the molecular level by self-limiting surface reactions [8] due to the alternate exposure of the substrate surface to different gas-phase reactants, known as precursors. The growth process continues by repeating so called ALD cycles, where a single cycle consists of the following steps:

a) The first gas phase precursor is carried by the carrier gas flow into the deposition chamber and reacts to form a (sub)monomolecular layer on the surface of a substrate onto which a film is to be deposited. The reaction will continue until surface is saturated (fig. 2 a), and the remaining unreacted precursors will start to be removed by introducing inert carrier gas.

b) Then any excess unreacted vapour of that reactant is pumped away by purging with inert carrier gas (fig. 2 b).

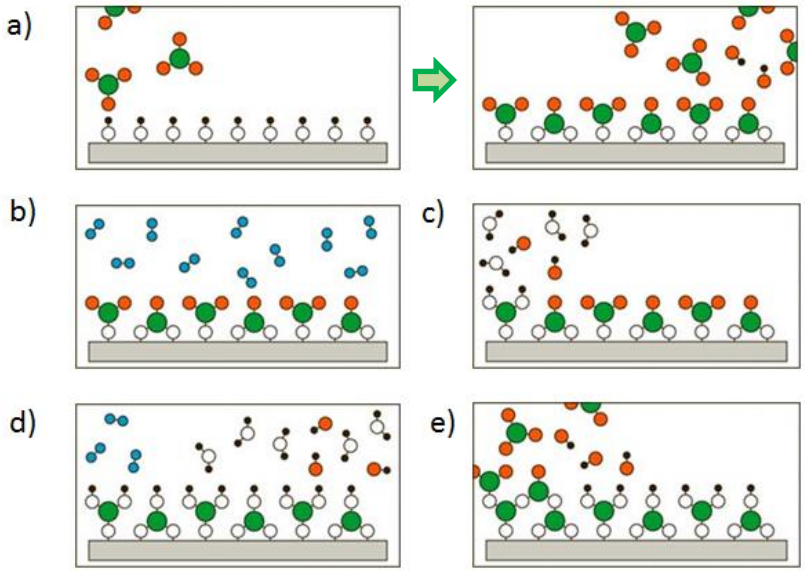

Fig. 2 Steps for a complete cycle in ALD process. a) A thin film layer is formed by the first gas phase precursor, b) unreacted vapour of reactant is pumped away c) the second reactant is brought to react with adsorbed surface species, d) remove of unreacted precursors by purge gas

c) Further, a vapour dose of the second reactant is brought to the surface. The new precursor will react with adsorbed surface species (fig. 2 c).

d) Purge with inert carrier gas is done in order to remove unreacted precursors.

With the above steps, an ALD "cycle" with the formation of no more than a single monolayer is completed. These cycles can be repeated to build up thicker films (fig. 2 e). Choosing of suitable precursors enables deposition of high-quality oxide, nitride, and metallic films [8].

1.3 Purpose of this study

The competitive pressure to produce "smaller, faster, cheaper" microelectronic devices means that reliability must be achieved using not only the minimum amount of material, but also the minimum amount of testing [1]. Minimum amount of testing means choosing of the most optimal measurement methods and instruments, which can give accurate and reliable results with the shortest possible time consuming, and also in the cheapest way possible.

Several measurement techniques, such as X-Ray Reflectivity (XRR), Transmission Electron Microscopy (TEM) etc., are used for characterizing thin films especially in terms of thickness and roughness determination [9, 10, 11]. Among the other advanced measurement techniques used in thin film measurement is Spectroscopic Ellipsometry (SE). It has become common technique for its advantages in fulfilling several important measurement requirements in thin film industry.

In this thesis Spectroscopic Ellipsometry (SE) will be highlighted as a suitable and reliable measurement technique for thin film thickness, refractive index (n) and extinction coefficient (k) measurement not only for single layers of thin film materials but also for multi-stacks of thin films especially grown by ALD technique. In addition, advantages of SE as a versatile tool for ALD technique will be stressed.

The main goal of this thesis was:

1. To prove the sensitivity of SE in thickness, refractive index, n, and extinction coefficient, k, for thin film material from 4 nm up to 20nm thickness range.
2. To study the optical properties (n, k) of TiO_2 and Ho_2O_3 single-layer thin film materials,
3. To show the ability of SE in characterizing multilayer laminated thin films in terms of thickness and optical properties for each layer, and further
4. To highlight the advantage of SE in determining the uniformity over the whole area of thin film material, grown especially by ALD.

Most of the experiments were carried out at Tartu University in Laboratory of Thin Film Technology by using SOPRA GES-5E ellipsometer and the sensitivity measurements were performed at Fraunhofer Institute for Photonic Microsystems (IPMS-CNT) in Dresden, Germany, using SOPRA EP-5 ellipsometer.

The results obtained during this thesis work have partially been published as posters at international conferences (Appendixes I and II) and formed a part of a scientific manuscript submitted to a peer-reviewed journal (Appendix III).

2. Ellipsometry method for optical properties characterization

2.1 Introduction to Ellipsometry

As is known widely (from Maxwell's theory) light is a wave represented by two mutually perpendicular vectors: **E**, the amplitude of the electric field strength, and **B**, the amplitude of the magnetic field strength, and both **E** and **B** are also perpendicular to the direction of propagation, z [fig. 2.1a]. The vector **E** is represented by a superposition of the two components, $\mathbf{E_x}$ and $\mathbf{E_y}$ (or p and s) that are orthogonal to the direction of propagation [fig. 2.1b] [12, 13].

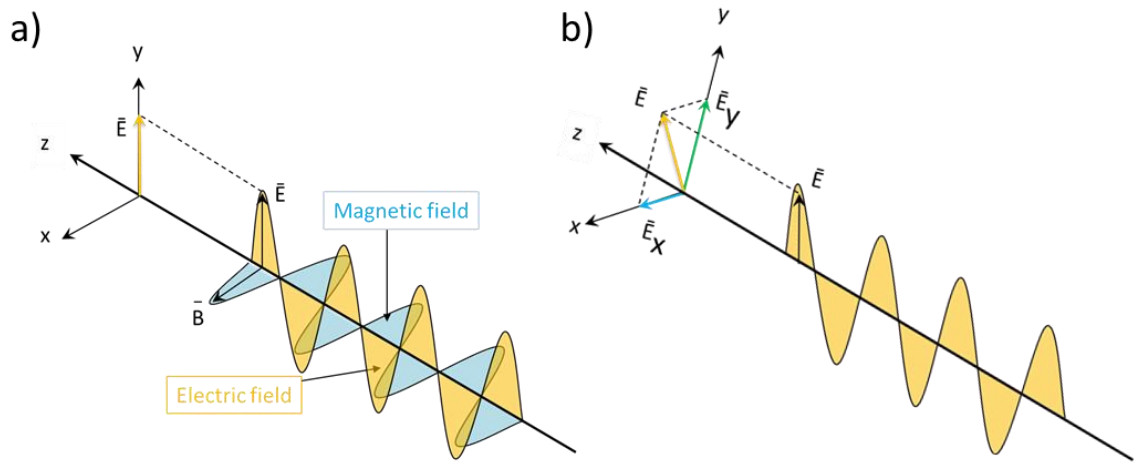

Fig. 2.1 Wave of light represented by a) electric (E) and magnetic (B) field components and, b) only electric field with superposition of two components $\mathbf{E_x}$ and $\mathbf{E_y}$

Ellipsometry measures the change in polarization state of light as it reflects or transmits from a thin film material structure [12]. The changed polarization state is represented as the amplitude ratio, Ψ, and the phase difference, Δ between p and s components of electric field of light (fig. 2.3). The measured polarization state depends on optical properties and thickness of the material in single or multilayer thin films under investigation (fig. 2.2).

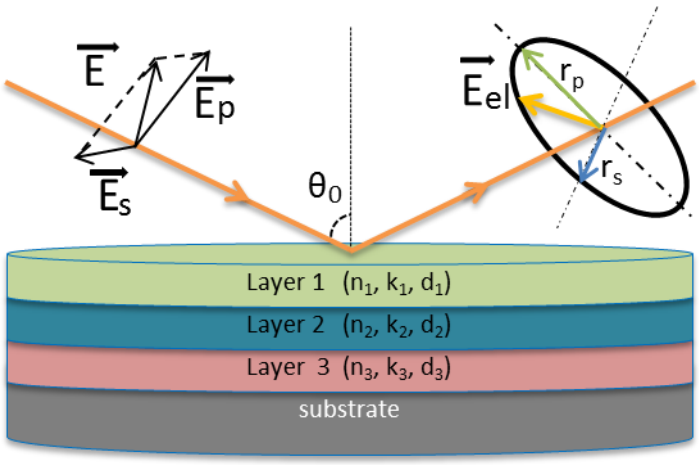

Fig. 2.2 Polarization state of light and optical properties in a multilayer thin film

Thus, ellipsometry is mainly used to determine film thickness and optical constants (refractive index, n and extinction coefficient, k) not only for single-layers but also for multi-layer thin films. However, it is also applied to characterize composition, crystallinity, roughness, doping concentration, and other material properties associated with a change in polarization state of light [14].

This chapter provides a fundamental description of ellipsometry method along with the measurement and typical data analysis procedure. The main advantages of ellipsometry versus other similar measurement techniques are also highlighted.

2.1.1 Principle of Ellipsometry

A beam of linearly polarized light, generated from a source of light, is irradiated onto a thin film surface at an incidence angle, θ. A part of light is reflected directly from the surface of sample while the other part of light is refracted (transmitted) into the sample structure. From a linearly polarized incidence light, an elliptically polarized light (from where the name 'ellipsometer' comes from) will take place after reflection from the sample material. Figure 2.3 shows the principle of ellipsometry.

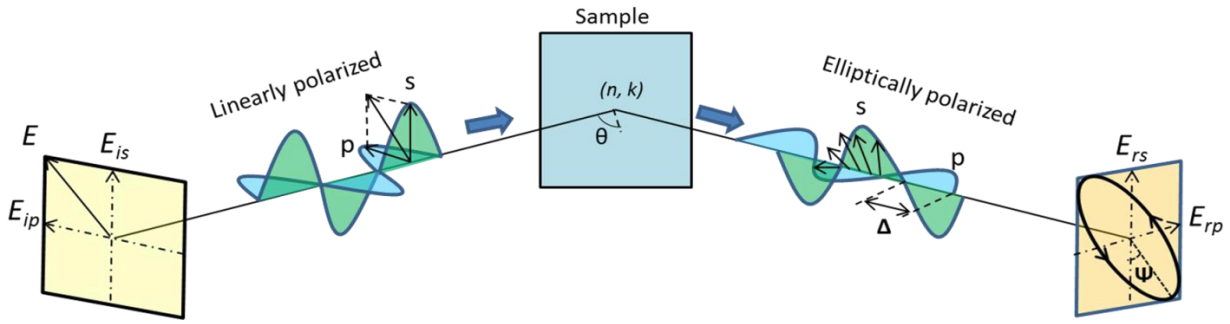

Fig. 2.3 Principle of ellipsometry

In ellipsometry measurement, the polarization states of incident and reflected light beams are described as p- and s-polarizations. The two components, p and s, of electric field of light, which are in phase (for linearly polarized light), emerge out of phase and show different change in amplitude after reflection from sample surface (for elliptically polarized light).

An ellipsometric measurement allows the determination of the phase difference, Δ, between reflected p- and s- polarizations of electric field of light and, tan Ψ which represents the change in the ratio of their amplitudes. In Fig. 2.3, Ψ represents the angle which is determined from the amplitude ratio between reflected p- and s- polarizations. For a bare reflecting surface, Ψ and Δ are in the form of:

$$\tan \Psi = \frac{|r_p|}{|r_s|}, \qquad (2.1)$$

$$\Delta = \delta_{rp} - \delta_{rs} \qquad (2.2)$$

Where, δ_{rp} and δ_{rs} are the phase changes and, r_p and r_s are originally defined by the ratios of reflected electric field to incident electric field for p and s components.

When light absorption from the film material is weak, the light waves are reflected at the film surface and film/substrate interface. In analysis of SE, thickness of thin films and multilayers are obtained from interference effect which appears when superposition of light waves, generated at different positions of a thin film formed on a substrate, occurs [fig. 2.4].

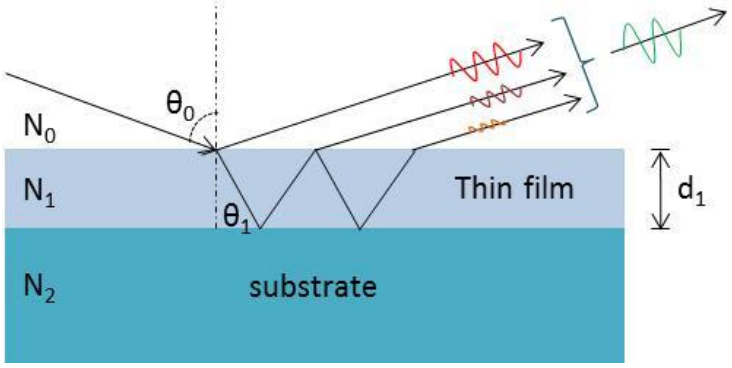

Fig. 2.4 Interference effect of light beams in a simple thin film material

As the light beam travels through the film material, a phase delay that is related to both the physical thickness and the complex index of refraction, N will occur.

In figure 2.4 is shown a simple example of a thin film layer grown on substrate. N_0, N_1 and N_2 represent refractive indices of air, thin film layer and substrate respectively. Each one is called a complex refractive index and is calculated as:

$$N = n + ik, \tag{2.1}$$

Where, n and k are refractive index and extinction (absorption) coefficient of material. In air ambient, n=1 and k=0, therefore N=1; θ_0, θ_1 and d_1 are incidence angle and, refraction angle of light from material and, thin film thickness respectively.

In figure 2.4, the wave amplitude becomes larger by this interference effect. Interfering beam will be considered as a single light beam with a certain polarization state, the exact nature of which is determined by sample's properties.

Thus, SE measurements contain information for thickness d, index of refraction n, and extinction coefficient k.

The expressions for r_p and r_s considering a single interface between medium 0 (ambient), with a complex refractive index N_0, and medium 1 (substrate), with a complex refractive index N_1 are as follows:

$$r_{01p} = \frac{E_{rp}}{E_{ip}} = |r_p| e^{(i\delta_{rp})} = \frac{N_1 COS\theta_0 - N_0 COS\theta_1}{N_1 COS\theta_0 + N_0 COS\theta_1}, \tag{2.4}$$

and,

$$r_{01s} = \frac{E_{rs}}{E_{is}} = |r_s|e^{(i\delta_{rs})} = \frac{N_1 COS\theta_0 - N_0 COS\theta_1}{N_1 COS\theta_0 + N_0 COS\theta_1} \quad (2.5)$$

While the total reflection coefficients (reflectance), for a film-covered (single) surface at the angle of incidence, θ_0 are:

$$R_p = |r_p|^2 \text{ and } R_s = |r_s|^2 \quad (2.6)$$

for p- and s- polarization components, respectively.

Which for multiple interfaces, (such as ambient/film/substrate) (fig. 2.3),

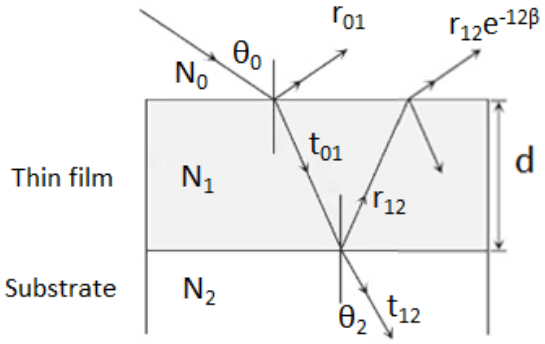

Fig. 2.3 Reflection coefficients in a ambient/film/substrate structure

are:

$$R_p = \frac{r_{01p} + r_{12p}e^{(-i2\beta)}}{1 + r_{01p}r_{12p}e^{(-i2\beta)}}, \text{ and } R_s = \frac{r_{01s} + r_{12s}e^{(-i2\beta)}}{1 + r_{01s}r_{12s}e^{(-i2\beta)}}, \quad (2.7)$$

Where, R_p and R_s are the total reflection coefficients for p and s components, respectively, and

β expresses the film thickness (d_1) and complex refractive index (N), at the wavelength of incident light λ, as follows:

$$\beta = 2\pi\left(\frac{d_1}{\lambda}\right) N_1 \cos\theta_0, \quad (2.8)$$

In the end, the polarization state of polarized light after reflection from sample's surface is characterized by following formula:

$$\rho = \tan(\Psi)e^{(i\Delta)} = \frac{R_p}{R_s}, \tag{2.9}$$

Which for the model in Fig. 2.3, ρ is obtained as a function of:

$$\rho = f(N_0, N_1, N_2, \lambda, d_1, \theta_0), \tag{2.10}$$

Where: N_0, N_1 and N_2 represent the refractive indices for the ambient, film and substrate, respectively, and R_p, R_s which are estimated based on reflection coefficients, (eq. 2.7).

In equation 2.10, usually, N_0, λ and θ_0 are known previously, N_2 can be independently obtained, and N_1 and d_1 are the parameters of interest which can be extracted from β (eq. 2.8) and β is obtained from equation 2.7.

2.1.2 Instrumentation basics

There are two major categories in where SE instruments can be classified: instruments with rotating optical elements and instruments with photoelastic modulator. Further, instruments with rotating optical elements can be classified into rotating analyzer ellipsometry (RAE) and rotating compensator ellipsometry (RCE) as illustrated in figure 2.3 [12].

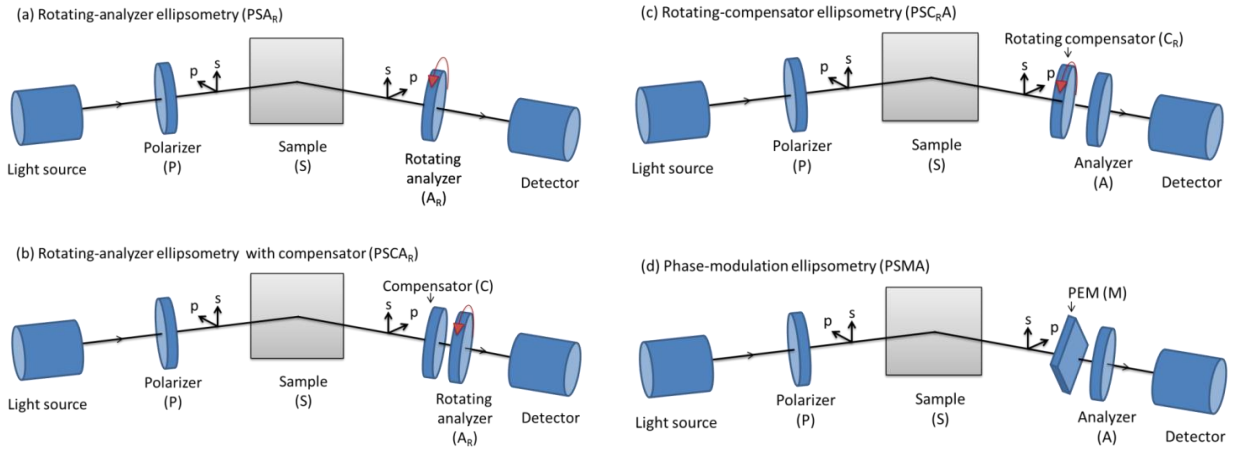

Figure 2.3 Optical configurations of ellipsometry instruments: (a) the rotating-analyzer ellipsometry (RAE), (b) the rotating-analyzer ellipsometry with compensator, (c) the rotating compensator ellipsometry (RCE), and (d) the phase-modulation ellipsometry (PME).

From the instruments classified above there are several distinctions which makes them different from each other. The main advantage of RCE and RAE with compensator is the capability of (Ψ, Δ) measurement over the full range. In particular, these instruments allow accurate measurements even when samples depolarize incident light.

A fast ellipsometry measurement and the capability for real-time measurement in the infrared region, are the major advantages of PME over the rotating-element ellipsometers. In contrast to PME, application of the rotating-element ellipsometers to real-time spectroscopic measurement is rather difficult in the infrared region.

Because ellipsometry measures the ratio of two values, it is highly accurate and reproducible and, because it measures a phase quantity 'Δ', it is very sensitive even to the presence of very thin film layers [14]. Except the feature of SE that it measures data at wavelength of interest, Variable Angle Spectroscopic Ellipsometry (VASE) provides new information because it allows to measure at different angle of incidence which optimizes sensitivity to unknown parameters.

2.1.3 Instrumental setup

The ellipsometer, shown in the figure 2.4, and used to carry out experiments described in chapter 3 of this thesis, is a GES-5E model of SOPRA core instrument for Research and Development (R&D) applications.

It has a high resolution goniometric bench by which the optimal measurement angle of any sample can be achieved known as Brewster angle [15].

Both the polarizer and analyzer arms of ellipsometer are mounted on a goniometric bench made of a double hollow crown (fig. 2.4). Both these crowns are driven by computer controlled stepper motors.

As a light source, a 75 W Xenon lamp is used, which emit a continuous spectrum of light, ranging from ultraviolet through visible to infrared (185 - 2000 nm). The spot size on sample at 75 ° angle of incidence is 3mm*12mm.

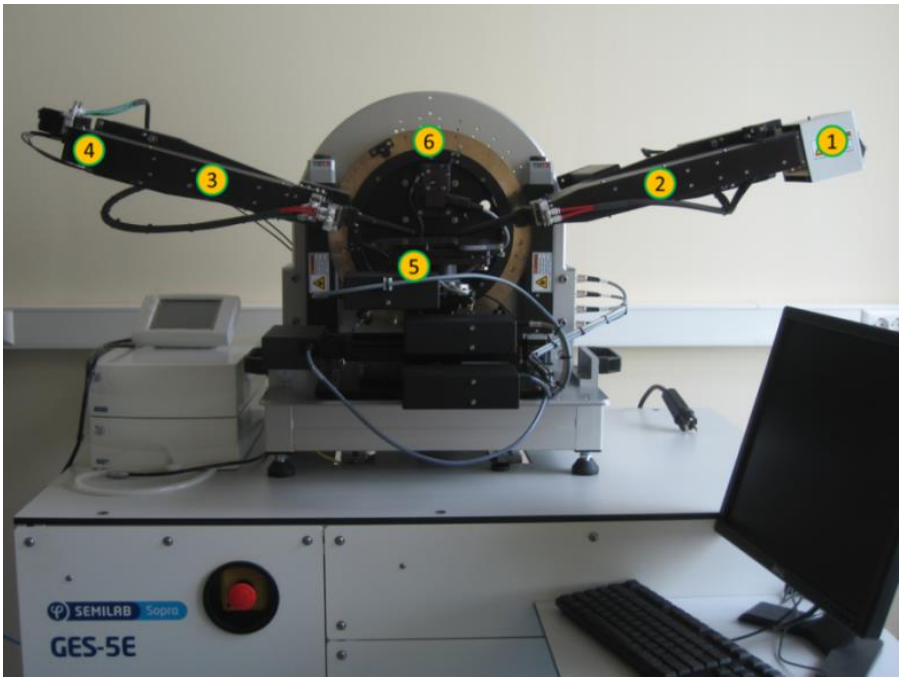

Fig. 2.4 The main physical parts of ellipsometer GES-5E instrument: 1. light source, 2. polarizer, 3. analyzer, 4. detector, 5. sample stage, 6. Goniometer.

The standard sample stage is located between the polarizer and analyzer goniometric bench. This stage is manufactured to accommodate standard sample dimensions of up to 200 nm in diameter but a 300 nm stage can also be supplied as an option [15].

The GES-5E ellipsometer (Fig. 2.4) is a Variable Angle Spectroscopic Ellipsometer (VASE) located at laboratory of thin film technology at University of Tartu. In this figure the main physical parts are noticed with numbers. A simplified schema of VASE is also shown and illustrated in figure 2.5.

The first arm (polarizer arm), at the entry, comprises a Polarization State Generator (PSG) coupled to a source of light. In all cases the PSG includes a linear polarizer set at an azimuth with respect to the plane of incidence.

The second arm, or exit arm, is used to determine the polarization of the out-coming beam. It comprises a Polarization State Analyzer, or PSA, and a detector. As a possible configuration to perform the spectral analysis in UV-VIS light, on a sample, serves a fast spectrograph with

Charge Coupled Device detector (CCD) which provides the solution in not only speed of measurement but also in a relatively high resolution.

The unique advantage of the GES-5E Platform is that the measurements are achieved with high resolution and the measurement spectrums are obtained in just a few seconds. In general the spectrum is obtained and analyzed as Ψ, Δ or tanΨ, cosΔ in a function of wavelength and angle of incidence.

GES-5E is widely used in research laboratories and universities working in the many fields, espedially in: Semiconductors, Optics, Flat Panel Displays, Data Storage, Thin Metals, etc. [7, 12, 13, 14, 16].

2.1.4 Ellipsometry measurements

The main instrumental parts of an ellipsometer are: light source, polarizer, sample, analyzer, and detector (fig. 2.5).

A light source (a xenon lamp in case of SE) produces unpolarized light which passes through a linear polarizer. The polarizer allows only a preferred electric field orientation of light to pass through while the polarizer axis is oriented between the p- and s- planes (noticed as wave 1 and 2 in figure 2.5), in such a way that both arrive at the sample surface.

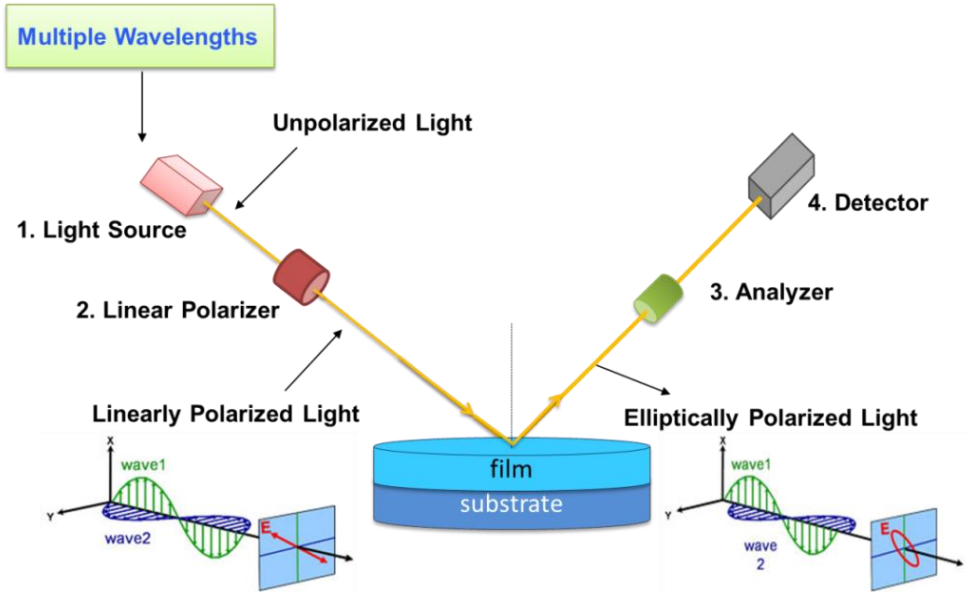

Fig. 2.5 The simplified schema with main instrumental components of a SE

The linearly polarized light becomes elliptically polarized after reflection from the sample surface, and travels through a continuously rotating polarizer (referred to as the analyzer). The amount of light which will go through the analyzer will depend on the exact elliptical polarization state of light coming from the sample. Further, a detector converts it to electronic signal to determine the polarization of reflected light. This information will be compared to the known linearly polarized input light to determine the polarization state changed by the sample's material reflection. This change in polarization is represented by values of tan Ψ and cos Δ (eq. 2.2, 2.3).

2.1.5 Data analysis

Even though SE is fast, non-destructive, and is very sensitive to changes in the film dielectric function perpendicular to the sample surface, the SE data requires mathematical analysis in order to calculate the parameters of interest, such as thin film thickness, surface roughness or the dispersion refractive index and extinction coefficient values versus wavelengths. In order to relate the SE-measured parameters with actual characteristics of the near-surface region, a model must be constructed, from which the Fresnel reflection coefficients (r_p and r_s) are calculated [17].

Data analysis usually is carried out into three steps. The first step consists on the construction of the optical model. The second step involves the parameterization or selection of the spectroscopic optical functions used in the model and the third step invokes a fitting procedure to determine the fitted parameters, their associated errors, and a measure of the 'goodness of fit' [17].

The procedure, used to extract material's properties from ellipsometry measurements is described in the following chart of Figure 2.6.

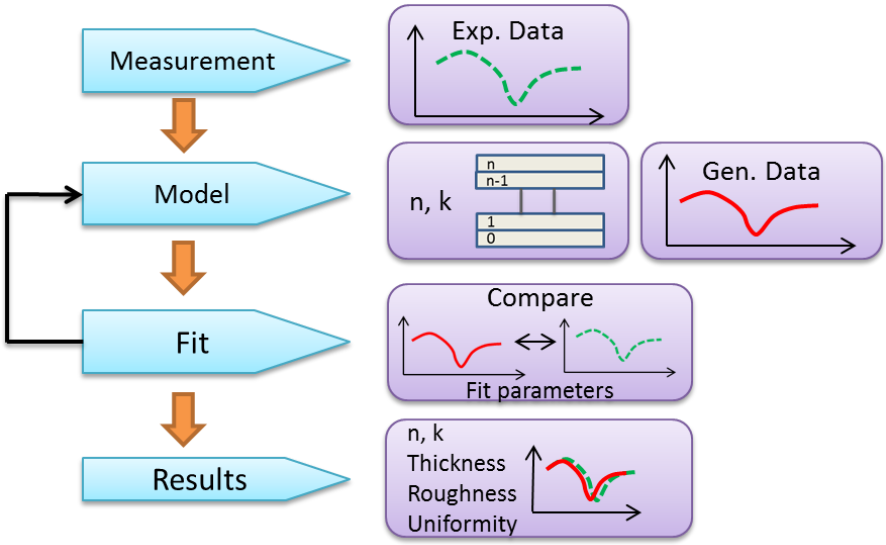

Fig. 2.6 Flowchart for ellipsometry data analysis

In more details, data analysis in the flow chart (figure 2.6) is interpreted as follows: After a sample is measured, using a computer, a model is constructed in order to describe the sample's optical properties. In construction of the model, assumed values of properties in interest are inserted and an optical dielectric function usually is employed to describe the dielectric properties of the sample's material. If the dielectric function of a sample is not known, it is necessary to construct it.

According to the optical properties of the sample it is necessary to select, among many dielectric function models, the appropriate one. There are several dielectric functions models, such as: Sellmeier, Drude, Cauchy etc. [12], which are used for different samples properties.

In transparent region ($\varepsilon_2 \sim 0$), for instance, Cauchy or Sellmeier [12] model is used. When there is free-carrier absorption, the data analysis is performed using the Drude model. This model is used to calculate the predicted response from Fresnel's equations which describe each material with corresponding thickness and optical constants. If these values are not known in advance, an estimate is given for the purpose of the preliminary calculation. Further, the generated values from the model are compared to experimental ones along with the all wavelength spectrum. The unknown material properties can then be extracted by varying the parameters themselves to improve the match between experimental and calculated spectrum. Further, the best match between the model and the experiment data is achieved only through regression analysis. An

estimator, like the Chi-squared Error (χ^2), is used to quantify the difference between curves. The unknown parameters are allowed to vary until the minimum chi-squared is reached. In the end, when a good fit is achieved, one can extract the parameters of interest such as: refractive index n, extinction coefficient k, surface and interface roughness, thickness and further uniformity, etc. [17].

2.1.6 Film thickness and optical constants

From the interference of light, which contains information for the amplitude and phase (eq. 2.1and 2.2), the film thickness is determined. While film thickness effect the path length of light which travels inside the film material, the index of refraction causes the change in velocity of the light wave by shifting the angle of refraction. This means that refractive index and thickness, both, causes the delay between interfering beams, which makes the light to become elliptically polarized. The polarization state is determined by equation 2.9. Further, the elliptically polarized light is analyzed and ellipsometric data (tan Ψ and cos Δ) are extracted.

As a thickness measurement technique, ellipsometry is used for films whose thickness varies typically from fraction of nanometers to a few microns. If films are thicker than tens of microns, interference oscillations become complicated to be analyzed [12]. In this case other characterization techniques are preferred instead. For thickness determination is also required that a portion of the light should travel inside the entire film and return back to the surface. Therefore, thickness measurement is often limited by high absorbance of materials [12].

2.2 Advantages of SE for thin films grown by ALD

The controlled deposition of ultrathin films is of fundamental importance for further development in thin film industry. 3D conformal deposition and control of film growth and material properties on the atomic level make ALD a very appropriate thin film deposition technique [7, 18].

Due to the natural link between material's properties and their effect in optical properties, in-situ SE is also used to monitor temperature, composition, crystallinity etc. in semiconductor industry [19].

Apart from the validity of SE as a tool for *in-situ* characterization of optical properties during ALD growing process, SE has traditionally been a more suitable method for *ex-situ*

measurements of thickness and optical properties of thin films grown by various methods including ALD.

To summarize, the major advantages of ellipsometry are:

- non-destructive method
- fast (full spectrum in a few seconds)
- sensitive due to small variations in thickness (up to 0.2 nm), and optical constants [14, 20]
- no need for specific sample preparation.

Furthermore, for many applications, as a fast and non-invasive technique, ellipsometry can be implemented to give results which are averaged over large areas and at much lower cost comparing to some other thickness measurement techniques (such as XRR, TEM, and Scanning Electron Microscopy (SEM) imaging for nanostructures) [14].

3. Experimental results

In this chapter, several experiments were carried out to show some of the main advantages of Spectroscopic Ellipsometry method. In the first experiment, sensitivity on very low thicknesses values (up to 4 nm) and sensitivity in refractive index changes due to change in ratio of chemical components of thin layer materials were performed by using a series of HfO_2 and a series of $HfZrO_2$ thin films, respectively. Further, in experiment 2 and 3, thickness, refractive index and extinction coefficient for single layer materials of TiO_2, Ho_2O_3 and for multilayer Ho_2O_3-TiO_2 laminate were studied. In addition a comparison of thicknesses values with other accurate measurement techniques is shown as a confirmation for reliable and accurate results provided by SE.

3.1 Experiment 1

The aim of this experiment was to prove the sensitivity of ellipsometry method, due to the small changes in thickness and refractive index values for very thin films.

In the first part of the experiment, a series of HfO_2 thin films grown by ALD with different numbers of cycles: 66, 100, 135, 200 and 335 nm at the same reactor conditions were measured. The experimental results are plotted versus the number or ALD cycles in the figure 3.4.

In the second part of the experiment, four samples of HfO_2 grown in the same conditions and with the same thickness, were analyzed to see the changes in refractive index due to change in amount of ZrO_2 added as a doping material.

Above mentioned materials were grown by ALD technique using a Crossflow design reactor (precursor flows across the substrate).

3.1.1. Sensitivity to thickness variations

Hafnium oxide[1] thin films were grown by ALD technique from $HfCl_4$ and H_2O as precursors, at substrate temperature of 300°C between two layers of TiN as shown in figure 3.1, (Appendix I).

[1] Hafnium oxide thin films used in this experiment were grown and measured in laboratories of Fraunhofer IPMS-CNT, Dresden, Germany.

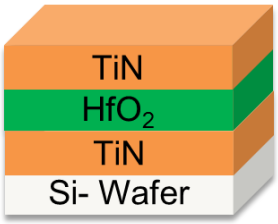

Fig. 3.1 HfO_2 thin film layer deposited by ALD at 300 °C, between two layers of TiN.

Thickness measurements, for each sample, were performed according the following procedure.

3.1.2 Measurement Procedure

a) Measurement of HfO_2 thin film

The measurement was performed using variable angle spectroscopic ellipsometer 'SOPRA EP-5' at incidence angle of 68° defined as Brewster angle [21]. In the whole range of wavelength, a series of measured data, tan Ψ and cos Δ, versus wavelengths of light (λ) were taken in a form of a spectrum, using software WinSE. Data analysis was performed using WinElli software.

b) Construction of an optical model

In construction of the optical model, in order to imitate the real thin film sample, a theoretical thickness was assumed, based on total number of ALD cycles, for each sample in series of HfO_2. As a standard dielectric function model for HfO_2 layer, Cauchy model [11] was chosen for the region of wavelength from 1.5 up to 4.5 eV and, Drude and Lorentz models for TiN layers. The initial values for all dielectric functions were taken from SOPRA library provided in the modeling software package. Since the TiN layer thicknesses were supposed to be the same in each sample's series, the optimized dispersion laws for n and k values constructed previously, were employed.

In a first attempt, an optical model including all layers was constructed (fig. 3.2a) which further was improved by adding interface layer of SiO_2 between substrate and bottom layer of TiN (fig. 3.2b).

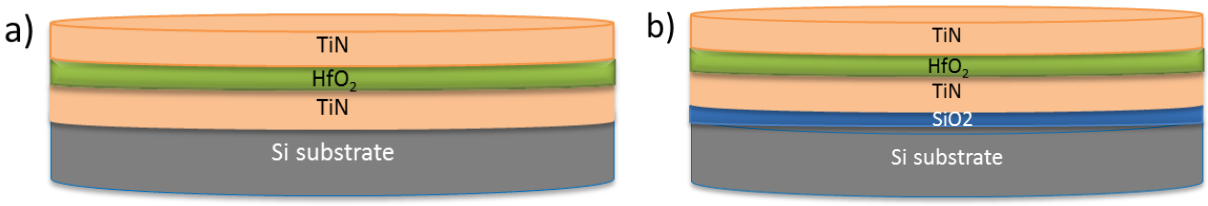

Fig. 3.2 Optical models of TiN/HfO_2/TiN multilayer thin film, a) without interface layer and b) including SiO_2 interface layer.

As dielectric function of SiO_2 interface layer was chosen n, k dispersions from the software's library.

c) Fitting spectrum and results

By using the previously constructed optical model, a fitting procedure was applied for both tan Ψ and cos Δ, parameter values versus wavelength (λ). In this fitting procedure, WinElli software was used and Levenberg-Marquardt regression was used as a standard technique to solve nonlinear least squares problems [22]. The fitted spectrum (fig. 3.3) was performed on a range between 1.5 and 4.5 electron Volt (eV) energy. The value R^2 is called 'coefficient of determination' which shows how well the theoretical data match with experimental ones.

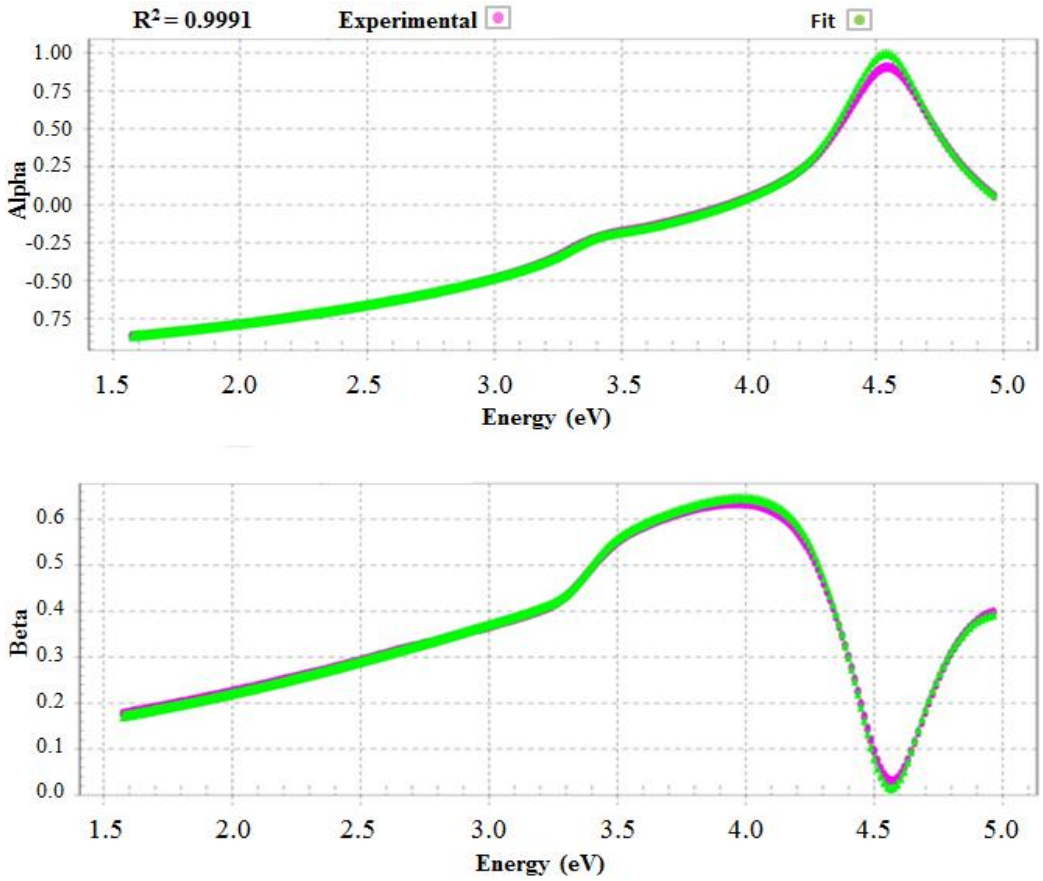

Fig. 3.3 Fitting spectra of experimental data (pink line) and fitting data (green line) for HfO_2 thin film layer using optical model in fig. 3.2b.

From regression analysis performed with optical model in fig. 3.2b, thickness values were obtained, for HfO_2 layers in each sample, which further were plotted in a graph (fig. 3.4), associated with error bars with standard deviation, versus number of ALD cycles applied in ALD growth process.

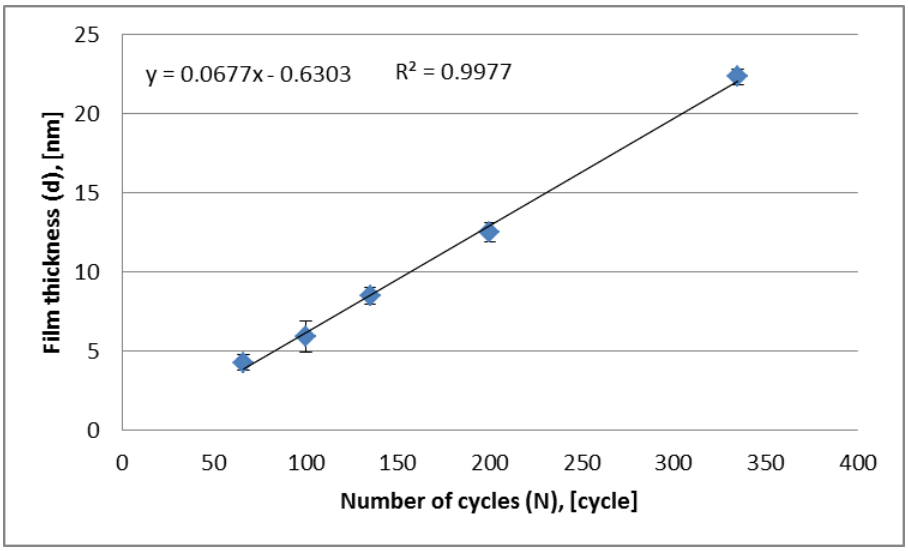

Fig. 3.4 Linearity between measured values associated with error bars of standard deviation, and amount of ALD cycles

From the graph in figure above, we can see that there is a linear relationship between the measured thickness values and number of ALD cycles in where, we can find the growth rate per cycle (GRC). GRC can be used to estimate the number of cycles necessary to be applied in an ALD growth deposition process to get a certain film thickness on the same conditions. GRC can also be used to estimate the theoretical thickness for a certain number of cycles applied during the ALD growth process.

$$d = GRC * N \tag{3.1}$$

Where, with 'd' is denoted thickness of thin film, 'N' is the total number of cycles applied in the growth process and 'R' is the growth rate taken from linearity of HfO_2 thin films.

Sensitivity to changes in refractive index

In this case, the growth temperature for samples of HfO_2 doped with Zr, was 450 °C and, cycles with precursors of $ZrCl_4$ and H_2O were combined with cycles of $HfCl_4$ and H_2O for achieving the needed concentration. The Zr/Hf ratios of the analyzed samples, estimated from number of cycles applied during deposition, were as described in table 3.1.

Tab. 3.1 Zr/Hf ratios of the samples used to investigate sensitivity in refractive index of SE.

Sample	Zr/Hf ratio
1	0:1
2	1:2
3	1:1
4	2:1

Experimental results for refractive index are plotted versus the above ratio Zr/Hf in percentage in figure 3.5.

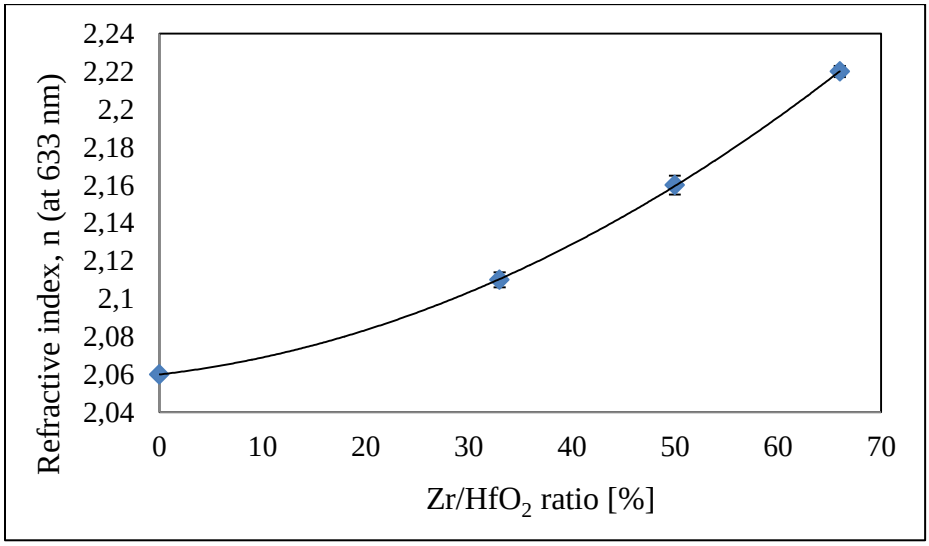

Fig. 3.5 Refractive index values plotted versus the Zr/Hf ratio and associated with standard deviations.

Since the ZrO_2 has a refractive index higher than HfO_2 (2.20 and 1.91 for ZrO_2 and HfO_2 respectively, according to WinElli software's library data referring to 633 nm wavelength), by adding more ZrO_2, it was expected an increase in refractive index values.

3.1.3 Conclusions and Discussion

The linearity, especially in the three last values (fig. 3.5), shows that ellipsometry is sensitive due to changes in ratio of materials with different refractive index values.

The shift to higher values of the experimental data compared to the initial reference values is because of the changes in process conditions, especially temperature which brings to changes in the degree of crystallinity of the material [21].

3.2 Experiment 2

Recently rare earth oxides, due to their interesting physical properties, have become very promising materials for use in various devices. Special interest have been shown in these chemical compounds for their technological application, as thin film capacitors, thin film transistors and insulating coatings in microelectronic devices, as protective coatings in optical coatings, etc. They exhibit high refractive index, good insulating and dielectric properties. Among these rare earth compound materials is holmium oxide (Ho_2O_3) [23].

TiO_2 is another material which has a large number of applications in electronic devices such as photovoltaic cells, gas sensors etc. [24]. TiO_2, as a semiconductor material, has many interesting properties. It is transparent in visible light, has high refractive index and low absorption which makes it widely used as an optical coating material [24].

In this experiment, among the physical properties mentioned above, dispersion characteristics for refractive index, n and extinction coefficient, k of Ho_2O_3 and TiO_2 thin films versus wavelength in a range from 0.2 to 2 μm will be shown. Furthermore, growth rates of those thin films have been extracted from measured thickness values and known number of cycles applied during ALD growth process.

In the third experiment a multilayer of Ho_2O_3-TiO_2 laminate thin film was studied [Appendix II and III]. In that case, thicknesses and refractive index values of constituent sub-layers have been on focus.

Ho_2O_3, TiO_2 and laminate of Ho_2O_3-TiO_2 thin films[2] were grown by ALD technique on silicon Si (100) substrate using a flow-type low-pressure ALD reactor. The measurements were performed using a variable angle spectroscopic ellipsometer (VASE) type GES-5E in UV/Visible light.

[2] Ho_2O_3, TiO_2 and laminate of Ho_2O_3-TiO_2 thin films were grown at Department of Chemistry in Finland and measured by SE at laboratory of Thin Film Technology in Institute of Physics in Tartu, Estonia.

3.2.1 Thickness and refractive index measurement – Ho_2O_3 and TiO_2

Sample description

Holmium oxide (Ho_2O_3) and Titanium oxide (TiO_2) thin films were grown by ALD with 1000 and 500 cycles respectively. Ho_2O_3 was grown with precursors of $Ho(thd)_3$ (thd = 2,2,6,6-tetramethyl-3,5-heptanedionato) and O_3 and, TiO_2 was grown with precursors of TTIP (titanium tetra-isopropoxide, $Ti(OCH(CH_3)_2)_4$) and O_3. Both thin films were grown at temperature of 300°C. Thickness and optical properties were studied using the procedure described below.

Procedure

a) Spectra measurement of Ho_2O_3 and TiO_2 thin films

The measurements were performed at 75° Brewster incidence angle [21], in a range between 1.55 and 5.0 electron Volt (eV) energy and a series of measured data psi (Ψ) and delta (Δ) versus wavelength of light (λ) were collected.

b) Construction of optical models

In order to construct an optical model which could imitate the real thin film sample based on total number of cycles, described on given recipe and growth rate reported on literature, (0.04 nm/cycle) [25], the initial thickness values were estimated using formula 3.1.

Simple optical models (fig. 3.6) were assumed with only one layer in the cases of Ho_2O_3 and TiO_2, on silicon Si (100) substrate.

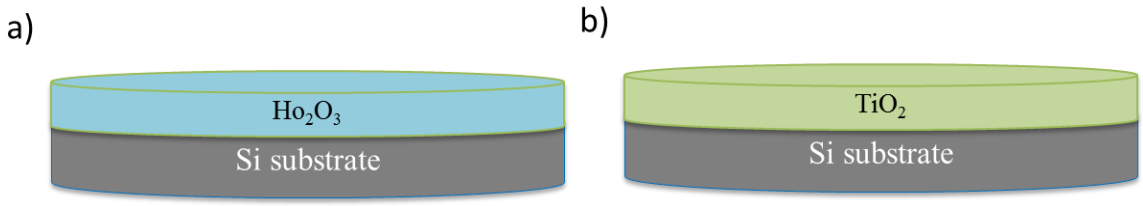

Fig. 3.6 Optical models with a) only one layer of Ho_2O_3, and b) only one layer of TiO_2.

Further, the optical models were improved by adding an interface layer of SiO_2 between thin film and substrate (fig. 3.7).

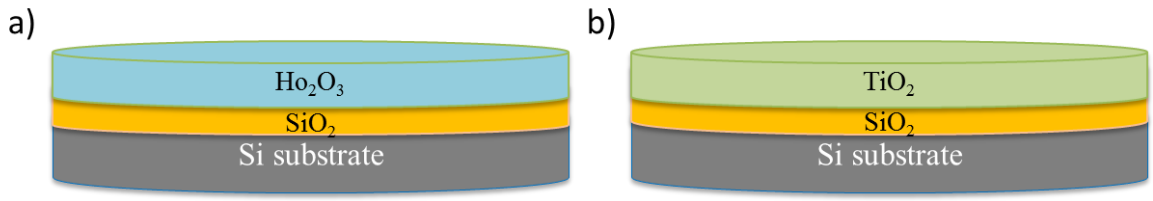

Fig. 3.7 Optical models with presence of SiO_2 interface layer in a) Ho_2O_3 and b) TiO_2 single layer thin films.

c) Fitting spectrum and results

Using the optical models of figure 3.7, a fitting procedure was followed for two parameter values, Ψ and Δ versus wavelength (λ).

From regression analysis performed with above mentioned optical models, refractive index, n and extinction coefficient, k values were obtained in a range of wavelength from 0.2 to 2.0 µm for both Ho_2O_3 (fig. 3.8) and TiO_2 (fig. 3.9) thin films.

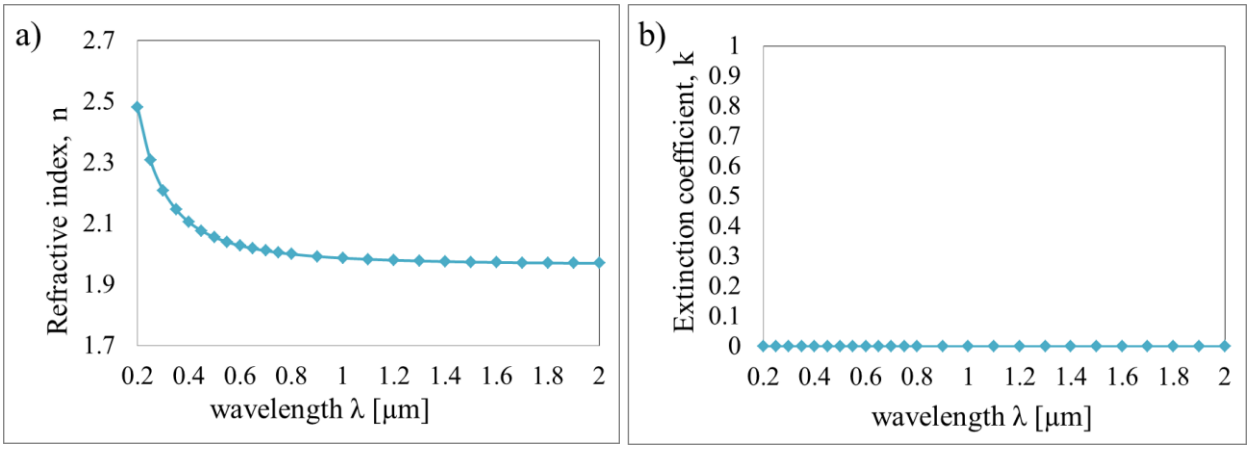

Fig. 3.8 Dispersion curves of a) refractive index and, b) extinction coefficient values on wavelength (λ) for Ho_2O_3 thin film

The dispersion curves of the refractive index, n (λ), and extinction coefficient, k (λ), presented above, are typical for Ho_2O_3 thin films [23]. The results, in figure 3.8-a and -b, show that despite the ultraviolet region, the refractive index dispersion exhibited is very small. Values of extinction coefficients seemed to be zero or at a level below possibility of detection. Such results for extinction coefficient for Ho_2O_3 values were also achieved in case of single layer study of Ho_2O_3 fabricated by the method of vacuum deposition with the help of an electron beam gun [23].

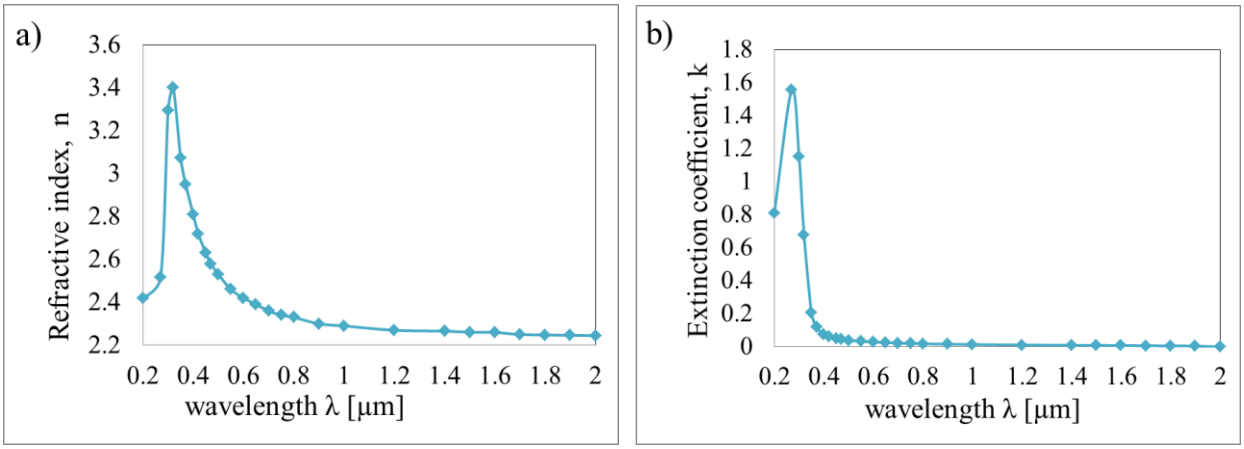

Fig. 3.9 Dispersion curves of a) refractive index and, b) extinction coefficient values on wavelength (λ) for TiO_2 thin film

The refractive index and extinction coefficient curves (fig. 3.9) are quite similar in shape with spectroscopic ellipsometry results of TiO_2 [26], with slightly increased refractive index value.

During the modeling, the Cauchy model was used as dispersion law which is described by equation,

$$n(\lambda) = A+B/\lambda 2+C/\lambda 2 \qquad (2.1)$$

Where, 'n' is refractive index, 'A, B and C' are fitting parameters.

Thickness results of ellipsometry were compared with XRR thickness values as presented in table 3.2.

Tab. 3.2 SE and XRR thickness results for optical models of fig. 3.7 a, and b.

Thin film grown on Si(100)	SE results [nm]	XRR results [nm]
Ho_2O_3	25.34 ± 0.62	24.6
SiO_2	1.67 ± 0.21	
TiO_2	22.19 ± 0.56	22.5
SiO_2	5.58 ± 0.42	

Based on above SE results, the growth rates using the formula 3.1 were found to be as shown in table 3.3.

Tab. 3.3 SE and XRR growth rate results based on nr. of ALD cycles and thickness results of Tab. 3.2

Thin film grown on Si(100)	SE Growth rate [nm/cycle]	XRR Growth rate [nm/cycle]
Ho_2O_3	0.025	0.025
TiO_2	0.044	0.045

Similar results of growth rate of single-layer films determined (using ellipsometry and confirmed by HRTEM), have been achieved and published by other authors to be 0.045 nm/cycle for TiO_2 [27] (APPENDIX III). Even though the results of SE match very well with XRR ones, it is important to mention that in case of SE measurement, the spot size is much more precise, stable and fixed at one angle of incidence while in case of XRR the spot size changes with angle of incidence.

3.3 Experiment 3

Nanolaminates are thin film materials composed of different alternating layers in thickness of nanometer scale. By changing the composition of layers, various thin film properties can be achieved [28]. While ALD is capable of producing parallel nanolaminations with precise control in thickness and uniformity [9], in this experiment, measurements for multilayer laminate Ho_2O_3-TiO_2 were carried out in order to prove the ability of SE in characterizing such properties.

3.3.1 Measurement of Ho_2O_3-TiO_2 laminated thin film

Sample description

Multilayer laminate Ho_2O_3-TiO_2 thin film was grown by ALD technique at temperature of 300°C using the cycle sequence: 10 x [100 x TiO_2 + 250 x Ho_2O_3] + 100 x TiO_2.

Measurement and data analysis of this multilayer film were performed in several steps due to its complicated structure comparing to single-layer thin films. The following procedure, explains in more details those steps.

3.3.2 Measurement process of multilayer Ho_2O_3-TiO_2 thin film.

In this case, several measurements have been performed at mainly 75° angle of incidence, at which a pair of psi (Ψ) and delta (Δ) data were obtained in each wavelength value from 1.5 up to 4.5 eV.

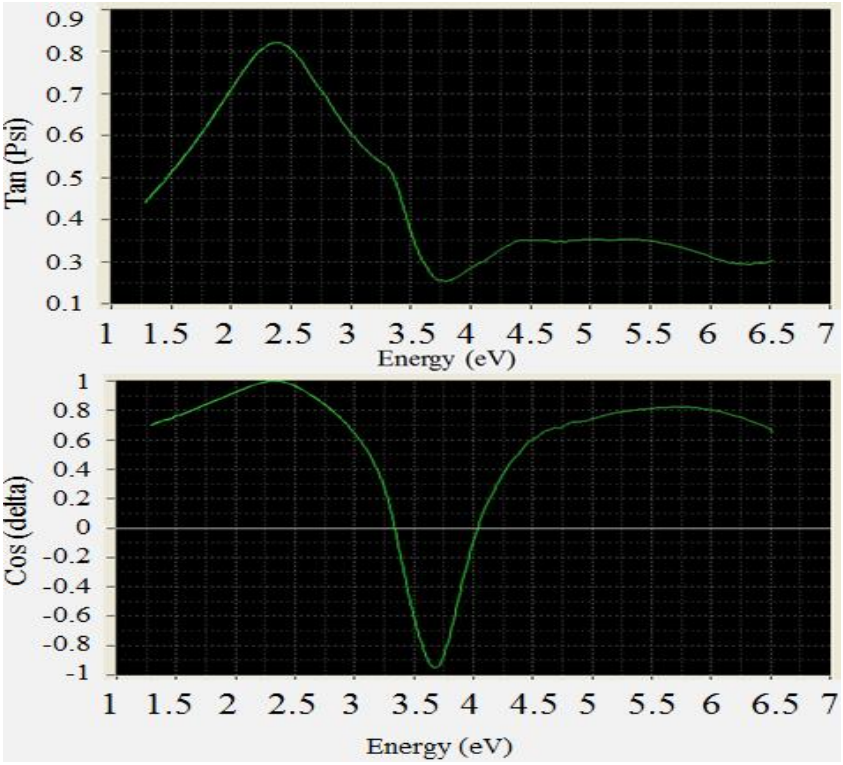

Fig. 4.0 Spectra of Ψ and Δ data obtained at 75° incidence angle plotted as tan(Ψ) (upper panel) and cos Δ (lower panel) versus energy in electron volts (eV)

In addition, using the same optical model (fig 4.1), measurement of thickness (d) were carried out over an area of 25 cm^2 on 49 points of multilayer laminate thin film with steps of 7 mm in both X and Y horizontal directions in order to profile the thickness along and across the gas flow direction in the ALD reactor.

3.3.3 Construction of optical model and fitting spectra

The dispersion models of figure 3.8 and 3.9, obtained from the single layer investigation in experiment 2, were extracted in the form of dispersion laws (n, k files), and further were used as dielectric functions to construct the optical model of multilayer laminate Ho_2O_3-TiO_2.

Primarily, simple optical models, concerning of two layers of Ho_2O_3 and TiO_2 were assumed by putting Ho_2O_3 above TiO_2 and vice versa (fig. 4a, b), and mixing of both layers together using Bruggeman mixing law (fig. 4c) [29].

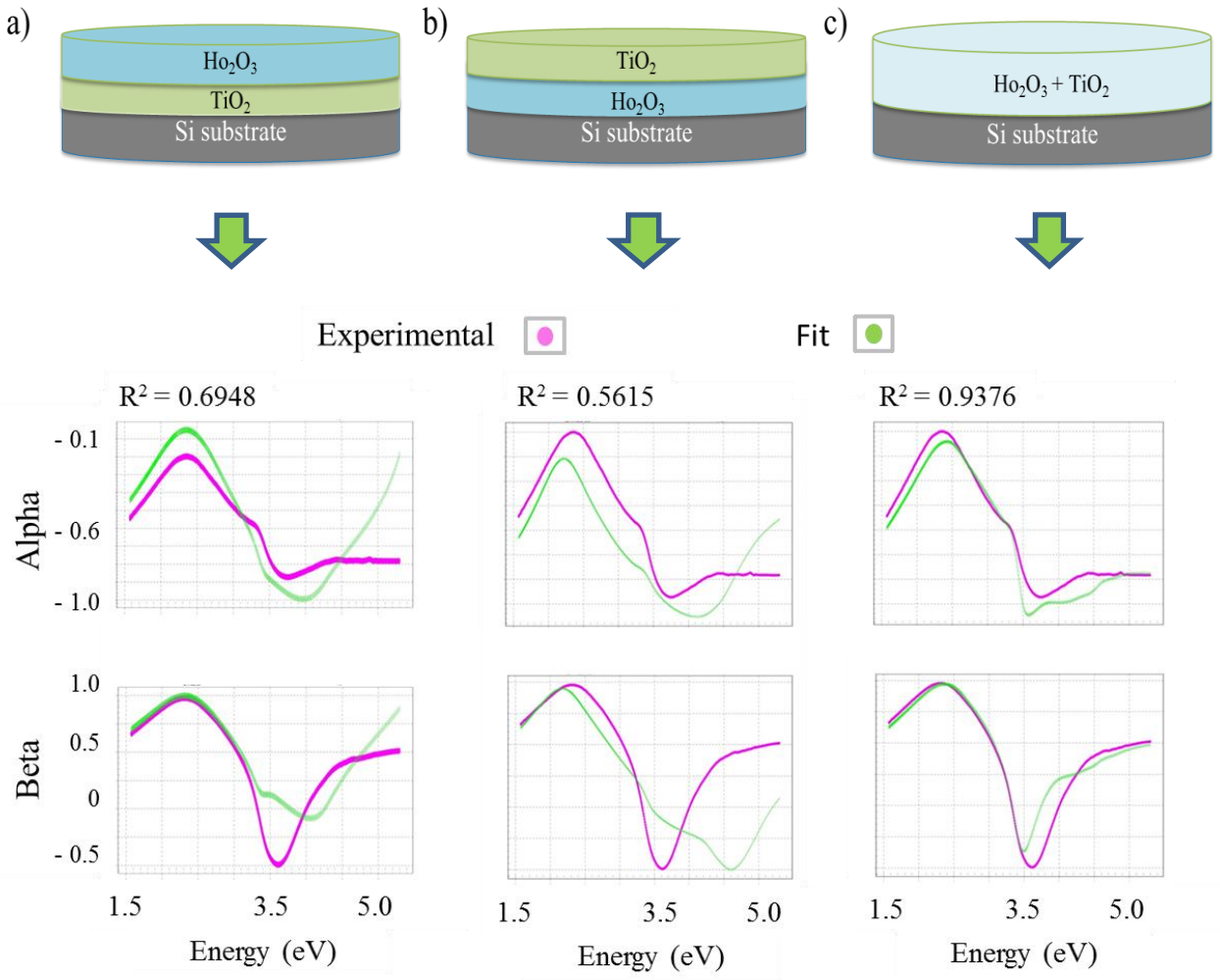

Fig. 4.1 Simple optical models for Ho_2O_3-TiO_2 nanolaminate structure concerning of a) Ho_2O_3 above TiO_2, b) TiO_2 above Ho_2O_3, and c) Bruggeman mixing of Ho_2O_3-TiO_2 along with spectral fittings respectively.

Further, a fitting procedure was applied, but the spectral fittings (fig. 4.1) were not good enough to rely on final results. The clear improvement of coefficient of determinations (R^2) in the case of mixing materials (fig. 4.1c), suggests that it is better to consider a more dispersion of two materials between each other. Several other models, considering more than two layers separated/mixed, were assumed but the results still remained unreliable.

Based on recipe of ALD growth process, (*10 x [100 x TiO_2 + 250 x Ho_2O_3] + 100 x TiO_2*) and on information provided by a HRTEM cross sectional image (fig 4.3), repeated units of the bilayer Ho_2O_3/TiO_2 were assumed in constructing of a 21 layers optical model, with an additional interfacial layer between the whole thin film and the substrate (fig. 4.2).

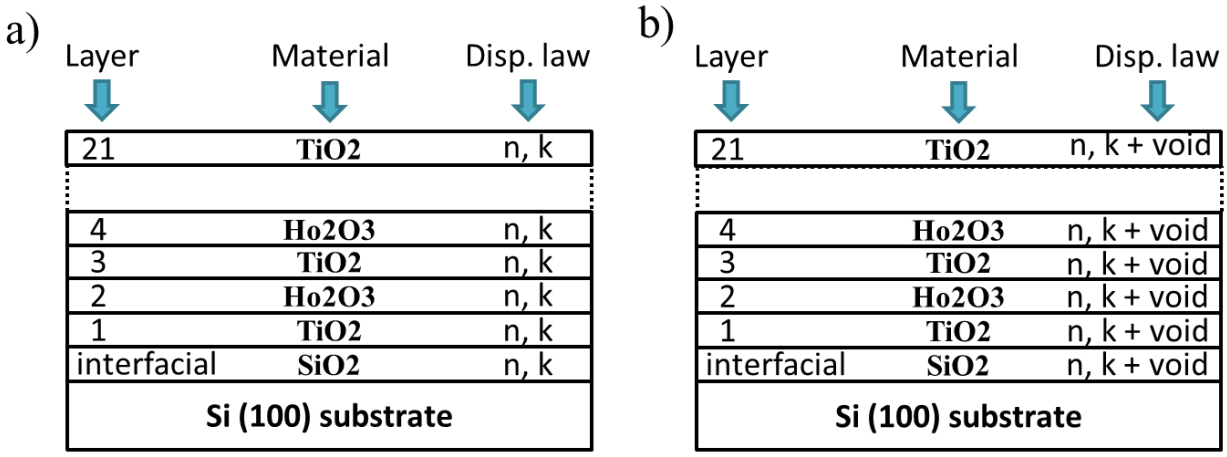

Fig. 4.2 Optical model for 21 layers for Ho_2O_3-TiO_2 laminated thin film used in a) thickness and b) refractive index adjustments during regression analysis.

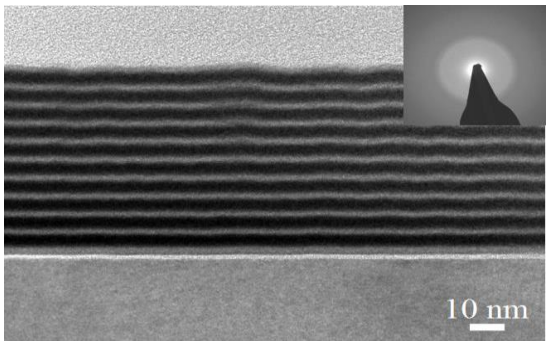

Fig. 4.3 Cross sectional image of multilayer Ho_2O_3-TiO_2 laminate thin film obtained using HRTEM technique.

As can be seen from the image obtained above, in our film there are 11 layers of TiO_2, and 10 layers of Ho_2O_3 with an interface layer of SiO_2 on silicon substrate.

The multilayer stack was modeled by fixing n and k for each layer (fig. 4.2a) to that of the corresponding single-layer films allowing variation of thickness throughout the layers. The initial thickness values were set at 6 and 4 nm for Ho_2O_3 and TiO_2 layers, respectively. By applying

regression analysis procedure from the beginning, thicknesses of layers were adjusted by leaving them as free parameters alternately between layers. After the results for thickness were almost stable, void contents were added to adjust the refractive index (n) and absorption coefficient (k) parameters. Negative void, in this context, refers to layers with higher refractive index than the reference material used in the model.

The regression procedure was continued by alternating thickness and refractive indices as free parameters until a good visually fit (fig. 4.4) was achieved with R^2=0.9986 and low value of $\chi^2 < 10^{-4}$ as statistical measure of Goodness Of Fit (GOF) parameter. The regression results for thickness and refractive index values referring to wavelength of 633 nm, in one of the measurement points are shown in figure 4.5.

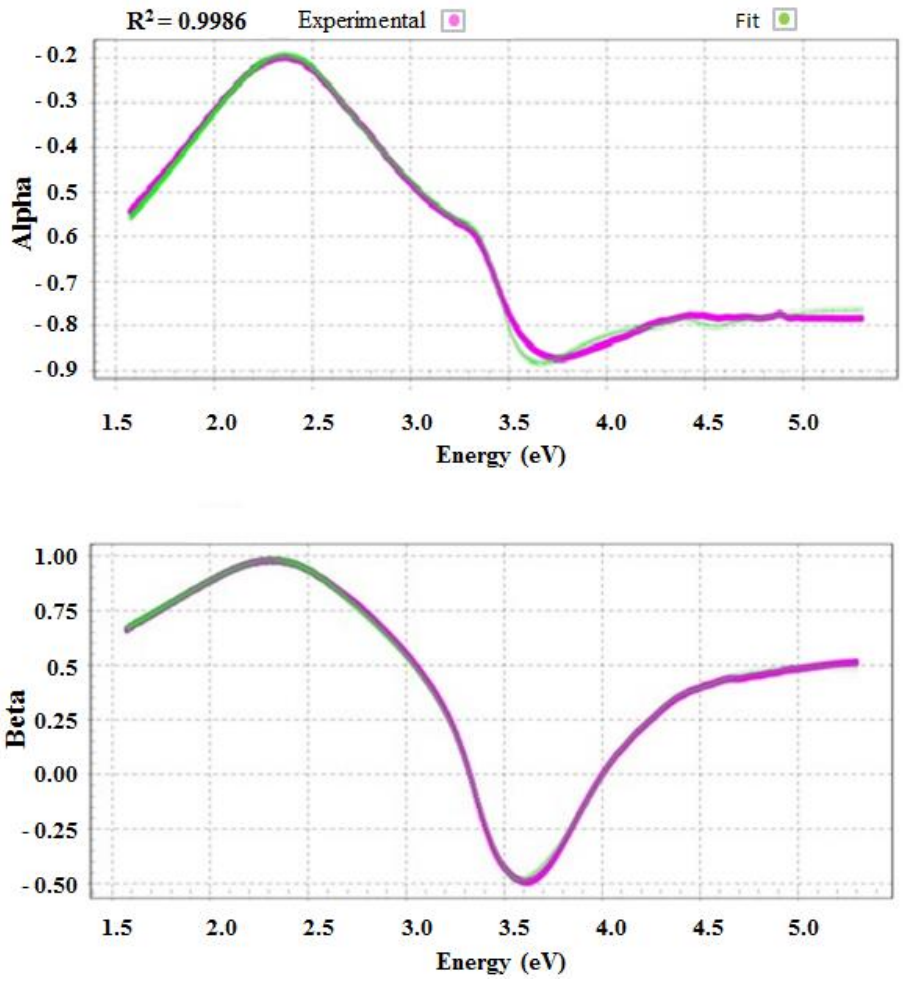

Fig. 4.4 Fitting spectra of laminate Ho_2O_3-TiO_2 thin film layer using optical model in figure 4.2

Since the fitted spectral matched with the experimental curves, the results obtained can be considered reliable.

3.3.4 Results and discussion

By relying on fitting spectrum obtained on figure 4.4 and HRTEM image on figure 4.3, it was possible to estimate thickness (d) and refractive index values (n) for each layer of laminate Ho_2O_3-TiO_2. Figure 4.4 shows results obtained from fitting in one of 49 measurement points on the laminate structure (Appendix II).

Fig. 4.5 Spectro-ellipsometric determination of both individual layer thickness, d (nm), and refractive index, n (λ=633 nm), of multilayer laminate Ho_2O_3-TiO_2 in one of 49 measured points

It was supposed to get higher values of thicknesses for each layer of TiO_2 and Ho_2O_3 based on theoretical calculations (growth rate and number of cycles) from single-layers.

There is a slightly increase of refractive index values in multilayer stack's results for Ho_2O_3 and TiO_2 (fig. 4.5) comparing to single-layer values of Ho_2O_3 (1.91) and TiO_2 (2.38), especially in the layers near to silicon substrate. The reason for such an increase in refractive index values

could be the densification of layers especially near to silicon substrate, as a result of increasingly longer time spent at temperature for layers deposited earlier in the process [9]. This phenomenon of densification can be also the main reason for such a reduction in thickness values.

Small variations in thickness may be caused as well due to errors in fitting procedure during data analysis process.

Thickness distribution over an area of 25 cm^2 was profiled as shown in figure 4.4.

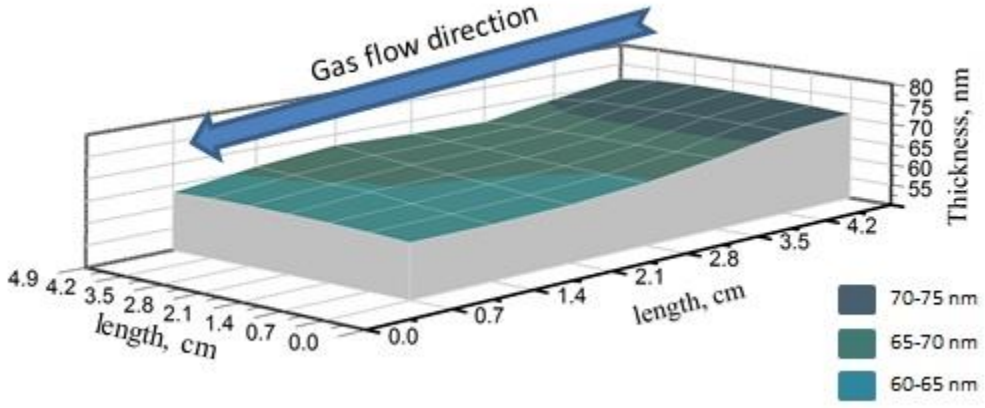

Fig. 4.6 Thickness profile of Ho_2O_3-TiO_2 multilayer thin film constructed from measurements carried out over an area of 25 cm^2, with steps of 7 mm in horizontal directions.

As we can see from fig. 4.4, there is a small variation of thickness values shown in vertical direction.

As we can see from fig. 4.4, there is a small variation of thickness values shown in vertical direction, where the thickness decreases with increasing distance from the reactor inlet.

The film thickness is often higher at the leading edge of the substrate, i,e, closer to the inlet of precursor gases, plausibly due to some overlap of the fronts and tails of the precursor pulses, and decreases towards the trailing edge of the substrate.

One reason for the cause of this phenomenon has been suggested to be reactions typical of Chemical Vapor Deposition (CVD). Another reason for such a thickness profile could also be secondary reactions between chemisorption reaction products and the solid surface [27].

4. Conclusions

1. Application of Spectroscopic ellipsometry (SE) technique has enabled accurate determination of film thicknesses and refractive indices of thin films.
2. In this thesis it was shown that SE is a very suitable measurement technique for atomic layer deposited thin films and probably thin films in general. SE is useful not only for single-layer films but also for multilayer-films consisting of multiple thin films alternately deposited.
3. By fixing refractive index values to those of single layer films, thicknesses of constituent layers can be obtained, and by adding void content in each layer, refractive index values are adjusted.
4. Accurate determination of film thicknesses and refractive indices for single and multilayer thin films, sensitivity to very thin films, uniformity determination etc., make SE a proper measurement tool for characterization of thin films in general and ALD thin film especially.

5. References

[1] David T. Read and Alex A. Volinsky, "Thin films in Microelectronics and Photonics," *Kluwer*, pp. 135–180, (**2007**).

[2] Mark T. Greiner and Zheng-Hong Lu, "Thin-film metal oxides in organic semiconductor devices: their electronic structures, work functions and interfaces," *NPG Asia Materials*, vol. 55, (**2013**)

[3] K. N. Chopra and A. K. Maini, "Thin Films and their Applications in Military and Civil Sectors," *Delhi -110 105*, India, (**2010**).

[4] K. Seshan, "Handbook of Thin Film Deposition: Processes and Technologies", *Elsevier/William Andrew*, Norwich, NY 13815, 2-nd edition (**2001**),

[5] M. Leskelä and M. Ritala, "Atomic Layer Deposition Chemistry: Recent Developments and Future Challenges," *Angew. Chem. Int*., vol. 42, pp. 5548–5554, (**2003**)

[6] L. Niinistö, M. Nieminen, J. Päiväsaari, J. Niinistö, M. Putkonen and M. Nieminen, "Advanced electronic and optoelectronic materials by Atomic Layer Deposition," *Phys. Stat. Sol.*, vol. 201, pp. 1443–1452, (**2004**).

[7] H. Kim, Han-Bo-Ram Lee, W.-J. Maeng "Applications of atomic layer deposition to nanofabrication and emerging nanodevices," *Thin Solid Films*, vol. 517 pp. 2563–2580, (**2009**).

[8] J. Päiväsaari, J. Niinistö, P. Myllymäki, C. Dezelah IV, C. H. Winter, M. Putkonen, M. Nieminen, and L. Niinistö, "Atomic Layer Deposition of Rare Earth Oxides," *Appl. Physics*, vol. 106, pp. 15–32 (**2007**).

[9] D. R. G. Mitchell, D. J. Attard, K. S. Finnie, G. Triani, C. J. Barbé, C. Depagne, and J. R. Bartlett, "TEM and ellipsometry studies of nanolaminate oxide films prepared using atomic layer deposition", *App. Surf. Sci*., vol. 243, pp. 265–277, (**2005**).

[10] L. Pereira, H. Águas, E. Fortunato, R. Martins, "Nanostructure characterization of high-k materials by spectroscopic ellipsometry," *App. Surf. Sci.*, vol. 253, pp. 339-343, (**2006**).

[11] Jebreel M. Khoshman, Martin E. Kordesch, "Optical properties of a-HfO_2 thin films," *Surf. Coat. Tech.*, vol. 201, pp. 3530–3535, (**2006**).

[12] H. Fujiwara, "Spectroscopic Ellipsometry: Principles and Applications", *John Wiley & Sons Ltd*, (**2007**).

[13] D. Gonçalves and E. A. Irene, "Fundamentals and applications of spectroscopic ellipsometry," *Quim. Nova*., Vol. 25, pp. 794 – 800 (**2002**).

[14] E. Garcia-Caurel, A. De Martino, J.P. Gaston, Li Yan, "Application of spectroscopic ellipsometry and Mueller ellipsometry to optical characterization," *Appl. Spectroscopy*, *v*ol. 2, (**2013**).

[15] User's manual GES5-E, SEMILAB SOPRA, http://www.semilab.com

[16] E.A. Irene, "Application of spectroscopic ellipsometry to microelectronics," *Thin Solid Films*, vol. 233, pp. 96–111, (**1993**).

[17] G.E. Jellison, Jr, "Data analysis for spectroscopic ellipsometry," *Thin Solid Films*, vol. 234, pp. 416–422, (**1993**).

[18] Booyong S. Lim, Antti Rahtu and Roy G. Gordon, "Atomic layer deposition of transition metals," *Nat. Mater.*, vol. 2, pp. 749–54 (**2003**).

[19] E. Langereis, S. B. S. Heil, H. C. M. Knoops, W. Keuning, M. C. M. van de Sanden, and W. M. M. Kessels, "*In-situ* spectroscopic ellipsometry as a versatile tool for studying atomic layer deposition," *J. Phys. D: Appl. Phys.*, vol. 42, 073001 (**2009**).

[20] B. M. Ayupov, V. A. Gritsenko, Hei Wong, C. W. Kim, "Accurate Ellipsometric Measurement of Refractive Index and Thickness of Ultrathin Oxide Film," *J. Electrochem. Soc.*, vol. 153, pp. 277–282, (**2006**).

[21] Jordi Sancho-Parramon, Mircea Modreanu, Salvador Bosch, Michel Stchakovsky, "Optical characterization of HfO_2 by spectroscopic ellipsometry: Dispersion models and direct data inversion", *Thin Solid Films*, vol. 516, pp. 7990–7995 (**2008**).

[22] M. I. A. Lourakis, “A brief description of the Levenberg-Marquardt algorithm implemented by levmar”, *Technical Report, Institute of Computer Science, Foundation for Research and Technology* - Hellas, 2005.

[23] T. Wiktorczyk, "Preparation and optical properties of holmium oxide thin films" *Thin Solid Films*, vol. 405, pp. 238–242, (**2002**).

[24] Hideki Takeuchi, Daewon Ha, and Tsu-Jae King, “Observation of bulk HfO_2 defects by spectroscopic ellipsometry,” *J. Vac. Sci. Technol.*, vol. 22, 1337 (**2004**).

[25] G. Triani, J. Campbell, P. Evans, J. Davis, B. Latella, and R. Burford, “Low temperature atomic layer deposition of titania thin films,” *Thin Solid Films*, vol. 518, pp. 3182–3189, (**2010**).

[26] Yujian Huang, Gregory Pandraud, and Pasqualina M. Sarro, “Characterization of low temperature deposited atomic layer deposition TiO_2 for MEMS applications,” *J. Vac. Sci. Technol.*, vol. 31, 01A148 (**2013**).

[27] H. Siimon, J Aarik, “Thickness profiles of thin films caused by secondary reactions in flow-type atomic layer deposition reactors”, *J. Phys. D: Appl. Phys.*, vol. 30, pp. 1725–1728 (**1997**).

[28] J.W. Elam, Z.A. Sechrist, S.M. George, “Zn/Al_2O_3 nanolaminates fabricated by atomic ayer deposition: growth and surface roughness measurements,” *Thin Solid Films*, vol. 414, pp. 43–55 (**2002**).

[29] A. Sihvola, “Mixing Rules with Complex Dielectric Coefficients”, *SSTA*, Vol. 1, pp. 393–415, (**2000**).

6. Summary in Estonian – Kokkuvõte: Spektroskoopiline ellipsomeetria aatomkihtsadestatud kilestruktuuride universaalse uurimisvahendina.

Spektroskoopiline ellipsomeetria on võimaldanud õhukeste aatomkihtsadestatud tahkiskihtide paksuse ja murdumisnäitaja määramist käesoleva töö eesmärgina. Magistritöö raames on näidatud, et ellipsomeetria on sobiv ja kiire meetod hindamaks nanomõõtmetesse sadestatud tahkiskihtide paksust, murdumisnäitajat ja kaudselt nende tahkiskihtide sadestamise kiirust. Töös uuritavate baasmaterjalide hulka kuulusid HfO_2, ZrO_2, TiO_2, TiN, Ho_2O_3. Tahkiskihtide paksusvahemik võib varieeruda mõnest nanomeetrist saja nanomeetrini, seega jäädes nanotehnoloogistesse piiridesse, mille juures uuritava objekti karakteristlik mõõde jääb alla 100 nm. Ellipsomeetriat rakendati selles töös *ex situ* meetodina. Töö jooksul on demonstreeritud ellipsomeetria sobivust mitte ainult ühest kindlast keemilisest ühendist koosnevate materjalikihtide analüüsimiseks, vaid ka kahest kuni kahekümnest erinevast materjalikihist koosnevate mitmikkihtide või supervõrelaadsete struktuuride uurimisel. Viimasel juhul on võimalik parameetreid valides ning murdumisnäitajate algväärtusi fikseerides usaldusväärselt hinnata erinevate koostiskihtide paksusi.

Töö jooksul saavutati mõningaid konkreetseid teadus-tehnoloogilist väärtust omavaid tulemusi, millistest osa on juba publitseeritud rahvusvahelistel konverentsidel ja/või saadetud avaldamiseks ISI WoK poolt indekseeritud teadusajakirjandusse. Demonstreeriti ellipsomeetria tundlikkust kõrge dielektrilise läbitavusega aatomkihtsadestatud tahkiskihtide optiliste omaduste analüüsil, näidates, et küllaltki lähedaste murdumisnäitajatega kondensaatormaterjalide, ZrO_2 ja HfO_2, segamisel $HfZrO_x$ tahkiskihis suureneb murdumisnäitaja märgatavalt koos Zr suhtelise osakaaluga kiles. Näidati, et optilise ja dielektrilise materjalina huvipakkuv aatomkihtsadestatud Ho_2O_3 absorbeerib valgust äärmiselt nõrgalt, olles seega praktiliselt läbipaistev. Demonstreeriti TiN-ZrO_2-TiN (kondensaatorstruktuur) ja TiO_2-Ho_2O_3-TiO_2-Ho_2O_3-TiO_2-…. (potentsiaalne multiferroiku baasmaterjal) nanolaminaatstruktuuride aatomkihtsadestuse ühtlust suurtel aluspindadel ja võimalust üksikute koostiskihtide paksuse ning tiheduse/murdumisnäitaja profileerimiseks planaarsetel alustel.

Õhukeste kilede ja nende multikihtide paksuste ja murdumisnäitajate täpse mõõtmise võimalus, üliõhukeste materjalikihtide detekteerimise võimekus, tundlikkus väikestele muutustele tahkiskihi paksuses ning murdumisnäitaja variatsioonidele on teinud ellipsomeetriast sobiva ja

efektiivse teadustöövahendi õhukeste kiledega seotud nanotehnoloogidele, sealhulgas aatomkihtsadestatud üliõhukeste, kuid suurepinnaliste kihtide analüüsiks.

7. Acknowledgements

I would like to express my sincere gratitude to Dr. Kaupo Kukli, for introducing me in the field of thin films and for his continuous support and very useful advices.

I would like to thank Dr. Aile Tamm very much for introducing me in the field of ellipsometry as well as for her polite instructions, useful advices, and investing so much of her time into teaching.

I would like to thank both of my supervisors for continuous encouragement and help especially in understanding of issues related with Atomic Layer Deposition thin films.

I sincerely acknowledge all my co-authors in the poster presentations and in the manuscript prepared for the introduction of the results of this work at international scientific forums.

This work was partially supported by Estonian Research Council (project PUT170).

8. APPENDICES

APPENDIX I

Poster presented at 12-th Baltic conference on Atomic Layer Deposition (BALD 2014), Helsinki, May 12-13, 2014

Spectroscopic ellipsometry as a versatile tool to study Atomic Layer Deposition (ALD) thin films

Roland Hoxha,[1] Aile Tamm,[1] Kaupo Kukli,[1,2]
[1] University of Tartu, Institute of Physics, Riia 142, EE-51014 Tartu, Estonia, e-mail: rolandi_ho@hotmail.com
[2]University of Helsinki, Department of Chemistry, P.O.Box 55, FI-00014, Univ. Helsinki, Finland

Introduction

In modern technology, in a variety of applications including semiconductor microelectronics, displays, optical filters, magnetic information storage and catalysis, thin films have to meet the demands for specific device requirements. Among these requirements are uniformity in thickness, conformality and thickness control.

While uniform conformal films can be successfully grown by atomic layer deposition (ALD), Spectroscopic Ellipsometry (SE) can be used as an accurate and fast measurement technique to provide correct and reliable results of these properties. In this study we have highlighted some advantages of SE in single and multi-stack thin films grown by ALD.

Principle

Spectroscopic Ellipsometry

A beam of linearly polarized light, generated from a source of light, is irradiated onto a thin film surface at an incidence angle θ. A part of light is reflected directly from the surface of sample while the other part of light is refracted (transmitted) into the sample structure.

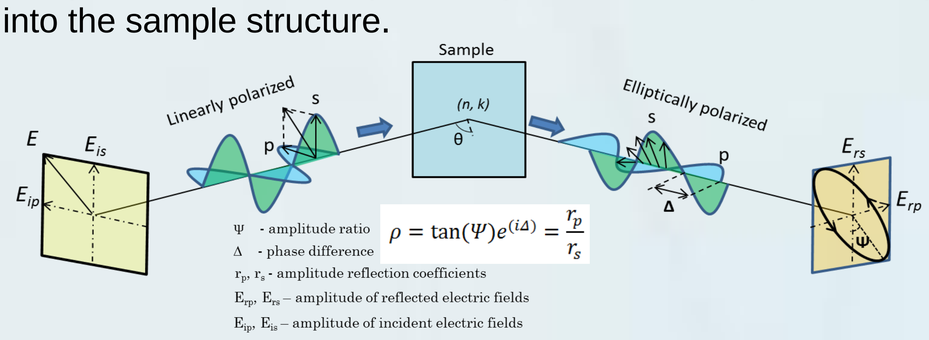

Every light beam which comes out of the thin film surface will be changed in polarization state. From a linearly polarized incidence light, an elliptically polarized light will take place after reflection from the sample material.

In a single layer thin film, when the light wave reflected from the surface (primary beam) overlaps with the light wave reflected at the film/substrate interface (secondary beam), an optical interference occurs.

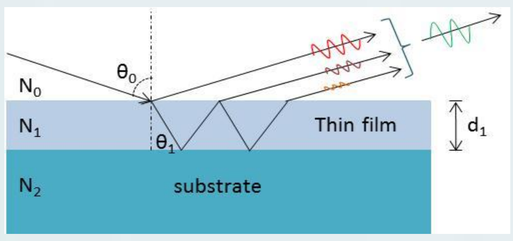

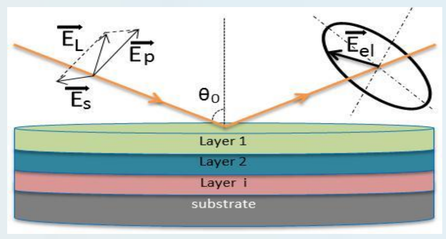

The wave amplitude becomes larger by the interference effect. Interfering beams will be considered as a single light beam with a polarization state, the exact nature of which is determined by sample's properties.

Instrumental setup

Instrumental setup of Ellipsometer GES-5E: 1. light source, 2. polarizer, 3. analyzer, 4. detector, 5. sample stage, 6. goniometer

Reference:

[1] Hiroyuki Fujiwara, Spectroscopic Ellipsometry Principles and Applications, John Wiley & Sons Ltd, 2007.

Advantages and applications

Illustration with experimental results

It is a non-contact and non-destructive measurement technique with a fast measurement and data acquisition. SE gives a full spectrum in a few seconds.

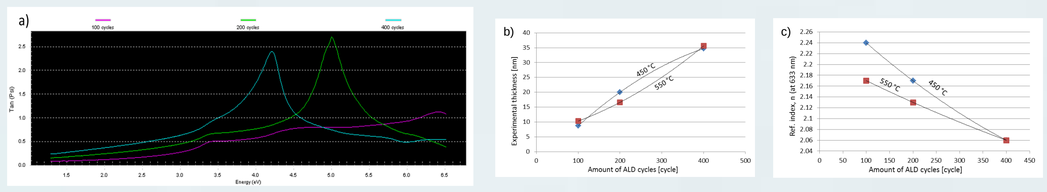

The measured spectra in SE for HfO_2 (with precursors of $HfCl_4$ and H_2O) at growth temperature (a) 450 °C and the measured values of SE for HfO_2 thin film at growth temperature of 450 and 550 °C for (b) thickness (c) refractive index, n.*

It has a wide application mainly in the field of scientific research (ex situ technique). It is very suitable for extraction of dispersion optical models of many materials.

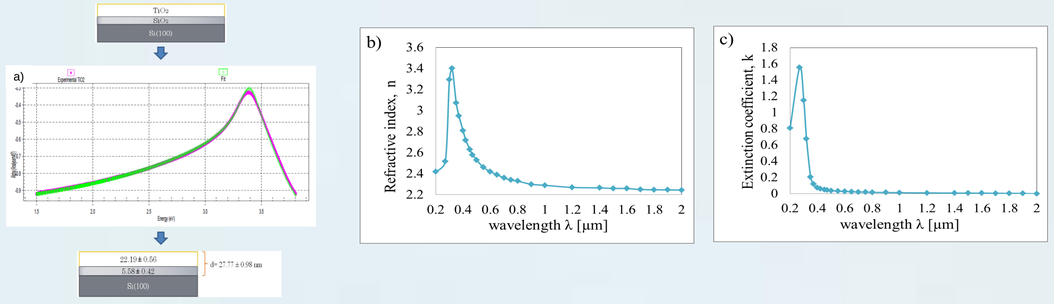

a) Optical model and fitting spectra for TiO_2 grown by ALD with precursors: TTIP+O_3, 500 cycles at 300°C. b) refractive index and c) extinction coefficient study of TiO_2.*

It is high sensitive due to the measurement of phase of the reflected light and can measure in the range from fractions of single layers to micrometers.

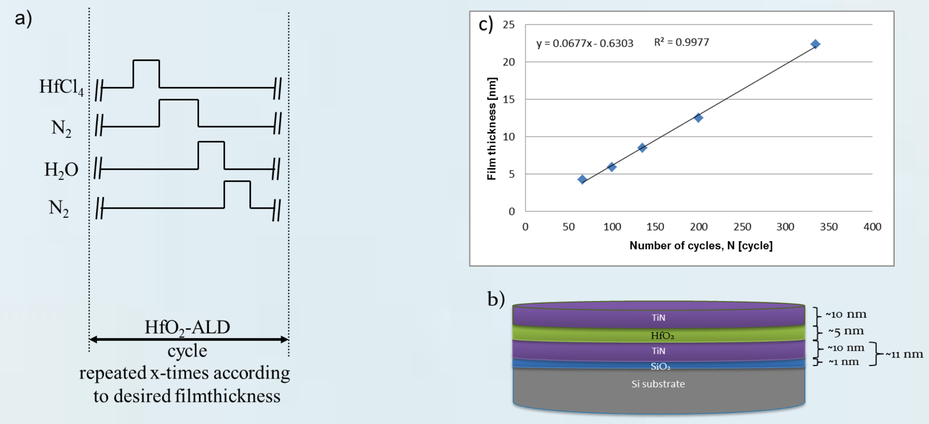

(a) precursors of HfO_2 thin film layer. (b) Theoretical model of HfO_2/TiN laminate. (c) linearity between measured values and amount of ALD cycles. Growth rate is determined by the slope of the line. **

The spot size of the light beam used in spectroscopic ellipsometry is typically several millimeters that means a low spatial resolution of the measurement. This allows uniformity measurement especially for ALD thin films.

Acknowledgements

This work was partially supported by Estonian Research Council (project PUT170) .

* Experiments carried out at Tartu University, Tartu, Estonia

** Experiments carried out at Fraunhofer IPMS-CNT, Dresden, Germany

APPENDIX II

Poster presented at European Materials Society Spring meeting 2014 (E-MRS 2014), May 26-30, Lille, France.

ATOMIC LAYER DEPOSITION OF HOLMIUM TITANIUM OXIDE THIN FILMS

Kaupo Kukli, Marianna Kemell, Esa Puukilainen, Mikko Heikkilä, Mikko Ritala, Markku Leskelä
University of Helsinki, Department of Chemistry, Finland
e-mail: kaupo.kukli@helsinki.fi

Jun Lu, Lars Hultman
Linköping University, Thin Film Physics Division, Linköping, Sweden

Joosep Link, Mukesh Chandra Dimri, Raivo Stern
National Institute of Chemical Physics and Biophysics , Tallinn, Estonia

Roland Hoxha, Aile Tamm
University of Tartu, Tartu, Estonia

MOTIVATION

Doped or mixed combinations of Ho_2O_3 and TiO_2 can be considered for

- substitution of dielectrics in transistors and capacitors,
- pH and biological sensors,
- materials able to photocatalytically split hazardous pollutants,
- multiferroics demonstrating both ferro-magnetic and ferroelectric properties.

This work studies the possibility to prepare holmium titanium oxide films at a low temperature by atomic layer deposition (ALD) process an provides their basic structural and magnetometric characterization.

EXPERIMENTAL

Precursors: titanium *tetra*-isopropoxide, $Ti(OCH(CH_3)_2)_4$; $Ho(thd)_3$ (thd = 2,2,6,6-tetramethyl-3,5-heptanedionato); and ozone, O_3

T_{growth} = 300 °C.

Substrates: SiO_2(1.5-2.0 nm)/Si(100)

ALD reactor: F120 (ASM Microchemistry Ltd.)

ALD cycle times: 0.5-0.5-1.0-0.5 s for TiO_2 and 1.0(or 2.0)-1.5-2.0-2.0 s for Ho_2O_3

RESULTS

List of selected films with ALD cycle numbers, thicknesses and Ho:Ti cation ratios measured by EDX.

cycles	thickness	Ho:Ti
1000 × Ho_2O_3	24.6 nm	—
350 × [1 × TiO_2 + 4 × Ho_2O_3] + 1 × TiO_2	49.0 nm	2.4
30 × [10 × TiO_2 + 50 × Ho_2O_3] + 10 × TiO_2	46.0 nm	2.1
400 × [1 × TiO_2 + 3 × Ho_2O_3] + 1 × TiO_2	39.0 nm	1.8
25 × [10 × TiO_2 + 35 × Ho_2O_3] + 2 × TiO_2	25.1 nm	1.5
700 × [1 × TiO_2 + 2 × Ho_2O_3] + 1 × TiO_2	33.0 nm	1.0
300 × [2 × TiO_2 + 5 × Ho_2O_3] + 2 × TiO_2	42.0 nm	0.8
40 × [2 × Ho_2O_3 + 20 × TiO_2]	27.5 nm	0.5
100 × [3 × Ho_2O_3 + 6 × TiO_2]	23.8 nm	0.5
50 × [5 × TiO_2 + 15 × Ho_2O_3] + 5 × TiO_2	17.0 nm	0.2
500 × TiO_2	22.5 nm	—

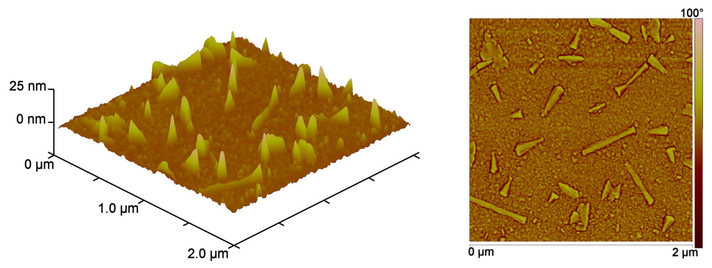

Atomic force microscopy topography (left) and phase (right) images of TiO_2:Ho_2O_3 films (EDX Ho:Ti = 2.4), annealed at 1000 °C in N_2 for 30 min

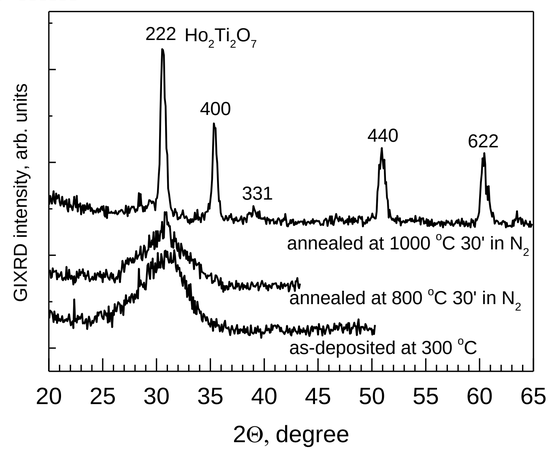

Grazing incidence X-ray diffraction results on nanolaminate TiO_2-Ho_2O_3 films grown using a sequence 10 x [100 x TiO_2 + 250 x Ho_2O_3] + 100 x TiO_2

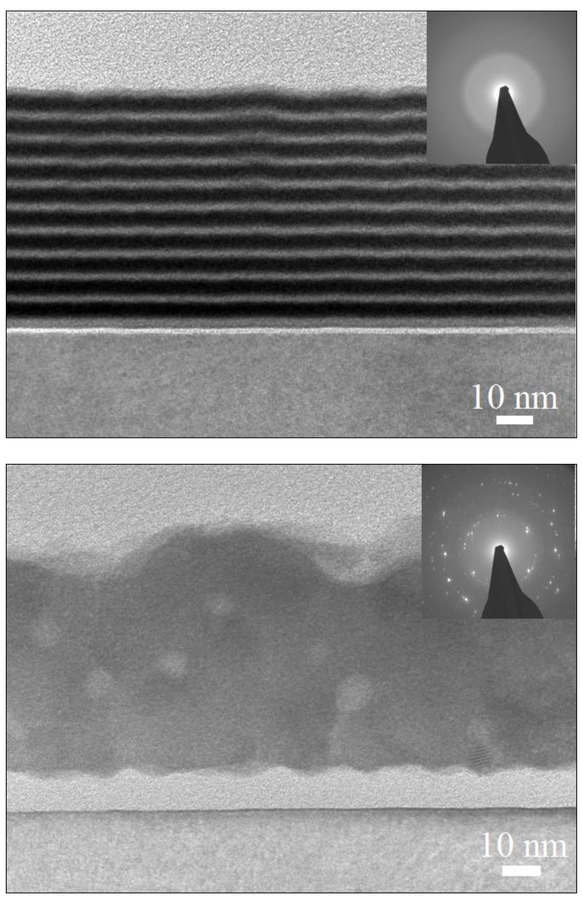

Transmission electron microscopy images from as-deposited (upper panel) and annealed (lower panel) nanolaminate TiO_2-Ho_2O_3 films grown using a sequence 10 x [100 x TiO_2 + 250 x Ho_2O_3] + 100 x TiO_2. Annealing was carried out at 1000 °C in N_2 for 30 min.

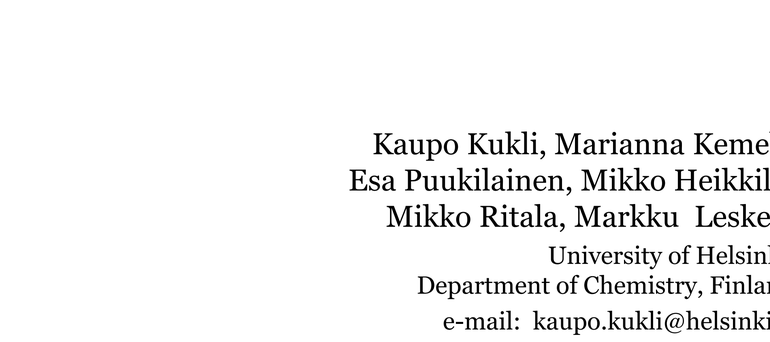

Lateral thickness profile from as-deposited nanolaminate TiO_2-Ho_2O_3 films taken over 5 x 5 cm² surface area using spectroscopic ellipsometry

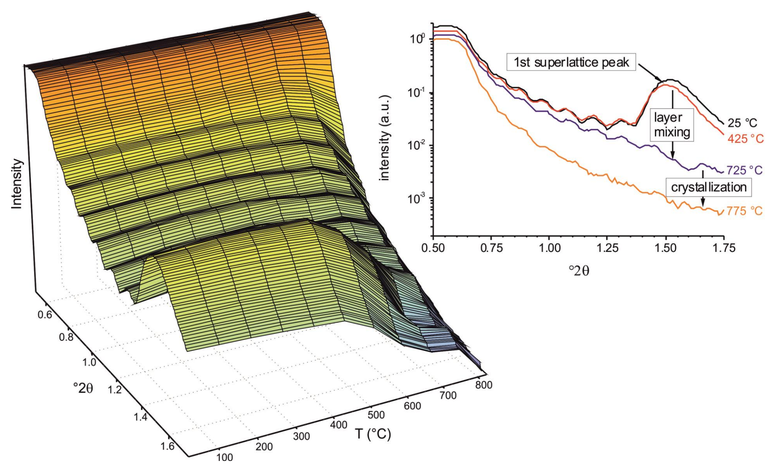

High-temperature X-ray reflectivity results on nanolaminate TiO_2-Ho_2O_3 films

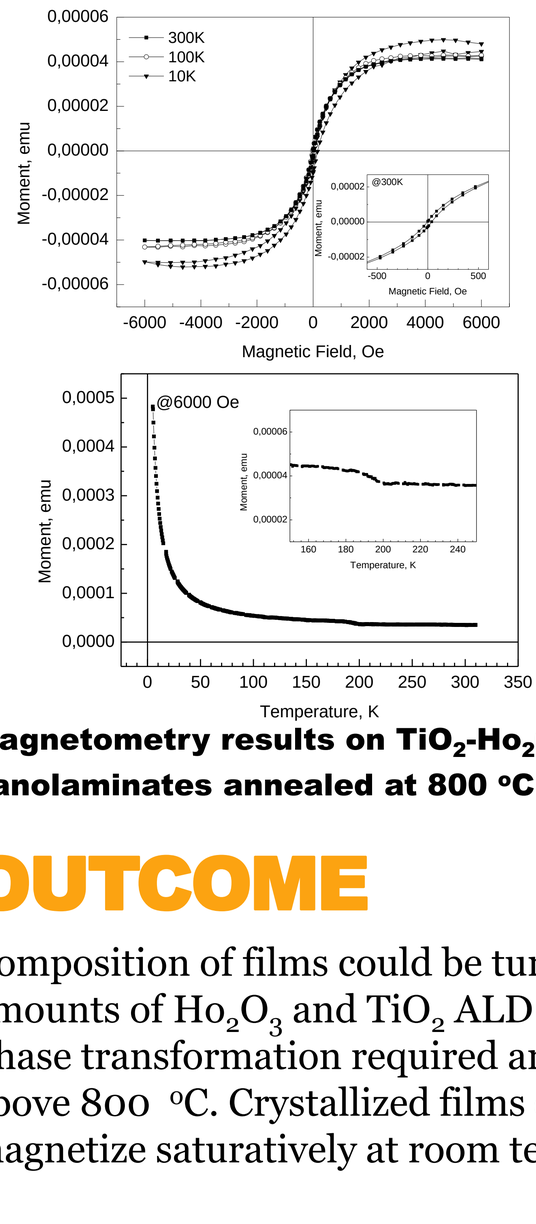

Magnetometry results on TiO_2-Ho_2O_3 nanolaminates annealed at 800 °C

OUTCOME

Composition of films could be tuned by the amounts of Ho_2O_3 and TiO_2 ALD cycles. Phase transformation required annealing above 800 °C. Crystallized films could magnetize saturatively at room temperature.

.

APPENDIX III

Manuscript submitted to Thin Solid Films, February 2nd 2014.

Holmium and titanium oxide nanolaminates by atomic layer deposition

Kaupo Kukli,[1,4] Jun Lu,[2] Joosep Link,[3] Marianna Kemell,[1] Esa Puukilainen,[1]
Mikko Heikkilä,[1] Roland Hoxha,[4] Aile Tamm,[4] Lars Hultman,[2]
Raivo Stern,[3] Mikko Ritala,[1] Markku Leskelä[1]

1) *University of Helsinki, Department of Chemistry, University of Helsinki, FI-00014 Helsinki, Finland; e-mail: kaupo.kukli@helsinki.fi*

2) *Linköping University, Department of Physics, Chemistry and Biology (IFM), Thin Film Physics Division, SE-58183, Sweden*

3) *National Institute of Chemical Physics and Biophysics, EE-12618 Tallinn, Estonia*

4) *University of Tartu, Institute of Physics, Department of Materials Science, EE-51014 Tartu, Estonia*

Abstract

Nanolaminate (nanomultilayer) thin films of TiO_2 and Ho_2O_3 were grown on Si(001) substrates by atomic layer deposition at 300 °C from alkoxide and β-diketonate based metal precursors and ozone. Individual layer thicknesses were 2 nm for TiO_2 and 4.5 nm for Ho_2O_3. As-deposited films were smooth and X-ray amorphous. After annealing at 800 °C and higher temperatures the nanolaminate structure was destroyed by solid-state reaction to form $Ho_2Ti_2O_7$. The films demonstrated diamagnetic or paramagnetic behaviour in the as-deposited state. After annealing, the films possessed net magnetic moment, allowing one to record saturation magnetization and weak coercivity.

1. Introduction

Metal oxide multilayers in the form of superlattices or nanolaminates are of interest as functional thin films possessing advanced electronic, optical and mechanical properties. Nanolaminates may be built up artificially by sequential deposition of different oxides, e.g. HfO_2-Al_2O_3 [1], ZrO_2-Al_2O_3 [2-6], ZrO_2-Y_2O_3 [7], ZrO_2-SiO_2 [7], HfO_2-Al_2O_3 [8,9], TiO_2-

Al_2O_3 [10-13], Al_2O_3–Ta_2O_5 [14-17], ZrO_2-Ta_2O_5[14,18], HfO_2-Ta_2O_5 [18,19], ZrO_2-HfO_2 [18,20], ZrO_2-Er_2O_3 [21], ZrO_2-Gd_2O_3 [22], and TiO_2-Cr_2O_3 [23].

Nanolaminates can assist in tailoring useful physical properties of different chemical compounds, such as band gaps, densities, refractive indexes, elasticity, homogeneity, or to exploit the formation of multiple interfaces as barriers for conduction or diffusion. Such oxide-based nanolaminates have been studied as materials able to provide good compromise between leakage current density and dielectric permittivity, enhancing charge storage capability of capacitor dielectrics while aiming at the improvement of the performance of, e.g., electroluminescent devices [10,14], field effect transistors [2,7,13,18,20] and memories [5,9,16,21,22]. Especially important industrially are the ZrO_2-Al_2O_3-ZrO_2 structures [24] used in dynamic random access memory cells. Nanolaminates may also perform as gas-diffusion barriers for reliable encapsulation of organic electronics [3], show long term durability as corrosion-protective layers [17], act as optical filters tuning the reflection from silicon substrate [11] or as hard X-ray mirrors [15]. Nanolaminates with large number of interfaces may also show reduced cross-plane thermal conductivity compared to that in chemically homogeneous films [1]. Alternate layering of different materials also reduces the overall roughness of the coating, compared to the single oxides grown to the same thickness [1,8,24,25].

Nanolaminates of single oxides may be grown using different physical and chemical techniques, such as electron beam evaporation [13], sputtering [4], pulsed laser deposition [6] or, as apparently the most controlled method, atomic layer deposition (ALD) [1-3,5,7,9-12,14-18,22-24,26]. Studies on ALD-grown nanolaminates containing rare earth oxides have so far been quite scarce, though.

This study is devoted to the description of Ho_2O_3-TiO_2 nanolaminates, grown by atomic layer deposition. Earlier, films consisting of mixtures of Ho_2O_3 and TiO_2 with variable Ho:Ti ratio have been grown by ALD [27]. The present paper will concentrate on stack of alternate Ho_2O_3 and TiO_2 films with controlled interlayer thickness. Effects of heat-treatment on the film morphology, crystal structure and magnetic properties will be presented and discussed. The study was initially motivated by the interest in the materials which could be deposited at low temperatures in a controlled way as structurally and optically well defined layers and,

either in the as-deposited state or after post-deposition treatment, exhibit magnetization, posssibly allowing further development of multiferroic materials.

2. Experimental details

The films were grown in a commercial flow-type hot-wall reactor F120 (ASM Microchemistry, Ltd.) [28]. The reactor run under a pressure of about 1000 Pa using N_2 (99.9995 %) as carrier and purging gas. O_3 was used as an oxygen precursor. The O_3 concentration output of the generator was ca. 100 g/m^3. Ho_2O_3 layers were deposited at 300 °C using the ALD process based on $Ho(thd)_3$ (thd = 2,2,6,6-tetramethyl-3,5-heptanedionato) and O_3 [27,29]. TiO_2 films were grown using an ALD process based on titanium *tetra*-isopropoxide, $Ti(OCH(CH_3)_2)_4$ and ozone, O_3. The titanium and holmium precursors were evaporated at 35 and 125 °C, respectively, from open boats inside the reactor and transported to the substrates by the carrier gas flow. The cycle times used for TiO_2 were 0.5-0.5-1.0-0.5 s, and those for Ho_2O_3 were 1.0-1.5-2.0-2.0 s, denoting the sequence metal precursor pulse – purge – O_3 pulse – purge. TiO_2-Ho_2O_3 nanolaminates were grown using the total sequence of $10 \times [100 \times TiO_2 + 250 \times Ho_2O_3] + 100 \times TiO_2$ cycles. The substrates were pieces of undoped Si(100) covered with 1.5-2.0 nm thick native SiO_2. Selected samples were annealed at 600, 800 or 1000 °C under a N_2 flow for 30 min.

High-resolution transmission electron microscopy (HRTEM) studies for characterization of the cross-sections of the nanolaminate structure were carried out using a FEI Tecnai G2 TF20 UT instrument with a field emission gun operated at 200 kV with a point resolution of 0.19 nm. The surface morphology images were taken and the film thicknesses measured by a Hitachi S-4800 scanning electron microscope equipped with an Oxford INCA 350 energy dispersive X-ray (EDX) spectrometer. The EDX spectra were measured at 20 keV. The beam current and spectrometer gain were determined from a calibration measurement performed under the same beam conditions. The film thicknesses and ratios of the different metals were calculated from the k ratios of Ho Kα and Ti Kα X-ray lines measured with the calibrated beam. The calculations were done with a GMRFILM program [30] assuming a density of 5 g/cm^3 for TiO_2 slightly doped and thus densified by holmium.

A Sopra GES-5E variable angle spectroscopic ellipsometer was used to determine the thickness (d) and optical properties (n, k) using 'Winelli II' software. Layer thickness and optical constants (n, k) were determined from the ellipsometric tan ψ and cos Δ parameters [40]. All the main parameters, d, n, and k parameters were obtained for each layer using a Levenberg-Marquardt non-linear regression algorithm. Measurements of were generally made at incidence and reflectance angles of 65°, 70° and 75°. Layers of Ho_2O_3 and TiO_2 were modelled as homogeneous mixtures of supposedly dense materials and addition of void content for refractive index, n, and absorption coefficient, k, adjustment. The optical properties of thin films were examined in air at ambient conditions. Optical constants quoted in this paper will further refer to those measured at 633 nm wavelength. In addition, using the same optical model, thicknesses were measured as a matrix laid over an area of 25 cm^2 with steps of 7 mm in X and Y horizontal directions in order to profile the thickness along and across the gas flow direction in the ALD reactor.

The thicknesses of the films were measured and their crystal structure evaluated by X-ray reflectometry (XRR) and by grazing incidence X-ray diffraction (GIXRD), respectively, using a PANalytical X'Pert PRO X-ray diffractometer with Cu K_α source. For the GIXRD, the incidence angle was set at 1 deg. For atomic force microscopy (AFM) studies a MultiMode V equipped with a NanoScope V controller (Veeco Instruments) was used. Tapping mode height and phase images were measured in air using phosphorus-doped silicon probe (RTESP) delivered by Veeco Instruments. Phase imaging detects e.g. variations in composition and it can be applied in order to map different components, such as amorphous and crystalline regions present in the material. Image processing and data analysis were performed with a NanoScope software version 7.30. The scan area was 2 μm × 2 μm and the Z-scale 25 nm in all the AFM images.

A selection of films was subjected to magnetic measurements. The measurements were performed using the Vibrating Sample Magnetometer option of the Physical Property Measurement System (PPMS) 14T (Quantum Design). Rectangular samples with dimensions of ca. 7 mm × 4 mm were fixed with GE vanish on commercial quartz sample holders (Quantum Design). The samples were cooled in a magnetic field of 6000 Oe parallel to the film surface and the temperature dependence of magnetization was measured in the temperature range from 10 to 310 K in the presence of the same field. The hysteresis measurements were performed by scanning the magnetic fields from – 477.6 kA/m to + 477.6

kA/m at temperatures selected in the range of 10–300 K. Diamagnetic signal arising from the silicon substrate was subtracted from the general magnetization curve for certain samples in which the ferromagnetic-like response was detected.

3. Results and discussion

3.1. Film growth and formation

3.1.1 Transmission electron microscopy

XRR measurements of thicker binary oxide reference films showed that the growth rate of Ho_2O_3 layers on SiO_2/Si substrates in these experiments was 0.025 nm/cycle. The growth rate of TiO_2 thin films was significantly higher, reaching 0.045 nm/cycle. These growth rates do not exactly correspond to the growth rate during the first few nanometers because the thicknesses of both Ho_2O_3 and TiO_2 single layers in the nanolaminate remained below the values expected on the basis of growth rates of reference films. The difference was more prominent in the case of TiO_2 than with Ho_2O_3. Figure **1** shows a cross-sectional TEM image taken from the nanolaminate in the as-deposited state. One can clearly see the periodical stack consisting of distinct Ho_2O_3 and TiO_2 layers. The thickness of the constituent layers in the laminate grown using the recipe $10 \times [100 \times TiO_2 + 250 \times Ho_2O_3] + 100 \times TiO_2$ cycles remained below 5 nm. EDX composition profile (Fig. **2**) from the nanolaminate further confirms that the film consists of chemically different alternating layers. Figures **1** and **2** also show that the layer interfaces remain relatively flat up to the top surface with a slightly accumulated roughness limited to less that one individual layer thickness (in the order of 1 nm).

3.1.2. Ellipsometry

Refractive indices measured from the reference single metal oxide films were 2.39 ± 0.02 and 1.98 ± 0.01nm, for TiO_2 and Ho_2O_3, respectively, at the wavelength of 633 nm. Growth rates for single layer films, deposited at temperature of 300 °C, were calculated to be 0.045 nm/cycle and 0.027 nm/cycle for TiO_2 and Ho_2O_3, quite well matching with the values obtained on the

basis of XRR mentioned above. Repeated units of the Ho_2O_3/TiO_2 bilayer were assumed in constructing a 21 layers optical model for the Ho_2O_3-TiO_2 nanolaminate, with an additional capping layer of TiO_2. The multilayer stack was modelled by fixing refractive index n and absorption coefficient k for each layer to that of the corresponding single-layer reference film allowing variation of the thickness throughout the layers by ~ 1 nm in accord with the TEM results (Fig. 1). Further, by adding void content into each layer, fitting of both thickness and refractive index was accomplished using the standard three-angle data sets. Fitting of the three-angle data sets and results as thickness (d) and refractive index values (n) for each layer are summarized in Fig. **3**.

The values of thicknesses for each layer of TiO_2 and Ho_2O_3 were preliminarily based on calculations taking into account the number of cycles. This kind of approach has also been applied earlier for the TiO_2 and Al_2O_3 layers forming respective nanolaminate structure [12]. Refractive index in TiO_2 layers was basically varying around the corresponding single layer value (2.39 at 633 nm). The refractive index values in both TiO_2 and Ho_2O_3 layers were quite stable throughout the multilayer stack indicating the stability of the growth and uniformity of the constituent layers [12,41]. Moderate variations in the layer thicknesses could be caused by errors in the fitting procedure.

Thickness distribution over an area of 5 x 5 = 25 cm^2 was measured as also shown in Figure **3** (the bottom panel). Obviously, the films grown were quite uniform with thickness deviation not significantly exceeding 10 % of the mean value. The nanolaminate occurred somewhat thicker close to the leading edge of the substrate and the thickness decreased steadily towards the trailing edge. This kind of thickness profile is rather common to ALD films grown in the particular flow-type reactor, and was also obtained in a study on the growth of TiO_2 from TTIP and H_2O [42]. The longitudinal thickness profiles may develop due to incomplete purging of precursors, secondary surface reactions or partial blocking of the surface adsorption sites from the precursors by the reaction byproducts [43].

3.2. Film structure and morphology

The reference 25-45 nm thick Ho_2O_3 and TiO_2 films were crystallized already in the as-deposited state. Ho_2O_3 films were crystallized to the cubic phase as observed earlier using similar precursor chemistry [29] whereas TiO_2 possessed anatase structure, also similarly to

that observed before, though using H_2O, then, as the oxygen precursor [42]. A recent study devoted to the mixing of Ho_2O_3 and TiO_2 and doping TiO_2 with Ho_2O_3 revealed that the crystallization temperature was significantly raised together with the Ho:Ti cation ratio approaching 1:1, i.e. that in $Ho_2Ti_2O_7$ [27].

The average Ho:Ti cation ratio measured by EDX in the TiO_2-Ho_2O_3 nanolaminate was 1.1. The composition of these films thus became close to that of stoichiometric holmium titanate. Similarly to the TiO_2-Ho_2O_3 mixture films, the nanolaminates remained X-ray amorphous in the as-deposited state, neither were they crystallized after annealing at 800 °C (Fig. **4**). In accord with HRTEM observations (Fig. **1**), some crystallization could be detected in Ho_2O_3 interlayers already in the as-deposited state, whereas the TiO_2 layers remained completely disordered. The crystallization in Ho_2O_3 layers was evidently not significant enough to become recognized by X-ray diffraction. Upon annealing at 1000 ^oC, the films became crystallized and the phase determined by XRD was $Ho_2Ti_2O_7$ (Fig. **4**). Signatures of Ho_2O_3 and/or TiO_2 were not detected in the patterns, neither were possible reflections from the perovskite $HoTiO_3$ [44] observed. The patterns were quite similar, regarding the most intense peaks, to those obtained earlier, e.g., for $Ho_2Ti_2O_7$ synthesized via solid state reaction of the component oxides [45] One can suppose that the ternary pyrochlore structure is energetically the most favoured and the easiest one to form, whereas the rest of the material remains amorphous or too weakly crystallized for X-ray diffraction.

In the sample annealed after deposition at temperatures ranging from 800 to 1000 °C the nanolaminate structure was destroyed. The originally distinct TiO_2 and Ho_2O_3 layers were mixed and the elemental composition map became homogeneous throughout the film thickness (Fig. **5**). One can see in the TEM images that the distinctive multilayer structure disappeared and, at the same time, round hollow-like features appeared, embedded in the host oxide film. The appearance of hollow regions might be attributed to the Kirkendall effect, i.e. the motion of the boundary layer between two metals or metal oxides due to the difference in diffusion rates of the cations. The Kirkendall effect can arise when two distinct materials are placed in contact to each other and their interdiffusion occurs by a vacancy mechanism. The Kirkendall effect can become observable by the formation of hollow regions, pores or voids during the diffusion process. These voids may accumulate vacancies and expand further in order to restore equilibrium in the material. Kirkendall effect is mostly observed in metal alloys, rather than in other materials such as mixtures of metal oxides. Nevertheless, there

exists, for instance, a study by Yang *et al*. [46], devoted to ALD of Al_2O_3 thin films on ZnO nanorods. After annealing the ZnO/Al_2O_3 core-shell layers were mixed and hollow $ZnAl_2O_4$ tube-like structures were controllably formed via Kirkendall process. It is thus possible, that ternary metal oxides, such as $Ho_2Ti_2O_7$ may form as a result of interdiffusion between the initially distinct regions of constituent binary oxides, i.e. Ho_2O_3 and TiO_2.

The nanolaminate in the as-deposited state possessed a smooth surface as revealed by AFM (Fig. **6**). The surface is clean and homogeneous, i.e. morphologically featureless. The average particle diameter can be estimated to be in the range of 20-30 nm. The rms roughness remains as low as 0.50 nm. As mentioned above, such films required annealing at least at 800 °C in N_2 for 30 min for the initiation of crystallization and were clearly transformed into crystallographically ternary phase upon annealing at 1000 °C. Naturally, the films also roughened upon annealing. Already upon annealing at 800 °C, features resembling particles, crystals or even bubbles were observed on the film surface (Fig. **6**). These round shaped features may correspond to the voids visible also in TEM figures. The surface features are different in size and shape, with the maximum height of ca. 30 nm, visible in both height and phase images. The density of these features varied from place to place on the surface causing also the rms roughness to vary between 0.7 and 1.6 nm.

The nanolaminate was also investigated by means of high-temperature X-ray reflectivity (Fig. **7**) which revealed the disappearance of nanolaminate structure and development of roughened, and evidently crystallized structure after the annealing. The temperature critical for the mixing of constituent layers in the laminate and consequent formation of the ternary holmium titanate obviously lies little above 700 ^{o}C

3.3. Magnetic behavior

Fig. **8** demonstrates magnetization in the as-deposited Ho_2O_3-TiO_2 nanolaminate on a Si substrate as functions of the measurement temperature and external magnetic field. One can see that a net magnetic moment could be measured in the sample at low temperatures but it decreased to zero already at about 100 K. In the ***M-H*** measurements, the nanolaminate did not show ferromagnetic behavior, but exhibited paramagnetic behavior at low temperatures, i.e. at 10 K. At room temperature the diamagnetic response overwhelmed the sample. This is not surprising, considering Ho_2O_3 and TiO_2 being paramagnetic and diamagnetic, respectivly, and

no additional phases like $Ho_2Ti_2O_7$ or $HoTiO_3$ were found in the as-deposited nanolaminates. In the sample annealed at 800 °C, i.e. after conversion of the clear multilayer to the more homogeneous structure, appearance of voids, and formation of ternary $Ho_2Ti_2O_7$ phase, the magnetization tended to saturate apparent in the whole temperature range examined. In accord with the measured magnetization-vs-temperature curve (Fig. **9**), the magnetization was measurable in the whole temperature range examined, and remained clearly above the zero around the room temperature as well. Certain transition was observed at 200 K. The transition occurred analogously to that observed earlier in double perovskites, such as epitaxial Bi_2CoMnO_6 synthesized by a solid state chemical route [47], La_2CoMnO_6 [48], or in laser ablated epitaxial La_2NiMnO_6 films [49]. The first magnetic transition at 180-200 K is incomplete as the drop in magnetization is rather weak. In the ***M*-*H*** curves, after substracting linear para- and diamagnetic components, saturation magnetization below 4.2×10^{-8} Acm^2 could be estimated at 300 K. The magnetization was very soft, with the coercive force not exceeding 4000 A/m. Saturative magnetization probably belongs to the already crystallized $Ho_2Ti_2O_7$, while paramagnetic contibution is due to the remaining amorphous phases. These in-plane magnetization loops were also similar to those observed earlier in double perovskites [47] and holmium titanates [45] in terms of their soft behavior.

Conclusions

Ho_2O_3–TiO_2 nanolaminates were grown by atomic layer deposition. Smooth films consisting of distinct metal oxide layers were formed, as recognized by microscopy and ellipsometric measurements. Post-deposition heat-treatment above 800 °C destroyed the multilayer structure but, on the other hand, led to the formation of a crystalline ternary phase, $Ho_2Ti_2O_7$. The films in which crystallization was initiated exhibited magnetic performance with saturative magnetization up to 5×10^{-8} $A\times cm^2$ and hysteresis within 3980 A/m in magnetization-versus-external magnetic field curves.

Acknowledgements

The work was supported by Finnish Centre of Excellence in Atomic Layer Deposition (Academy of Finland), Knut and Alice Wallenberg Foundation (Sweden), and research projects IUT-24 and PUT170 (Estonian Research Agency).

References

[1] N. T. Gabriel, J. J. Talghader, Thermal conductivity and refractive index of hafnia-alumina nanolaminates, J. Appl. Phys. 110 (2011) pp. 043526.

[2] W.F.A. Besling, E. Young, T. Conard, C. Zhao, R. Carter, W. Vandervorst, M. Caymax, S. De Gendt, M. Heyns, J. Maes, M. Tuominen, S. Haukka, Characterisation of ALCVD Al_2O_3–ZrO_2 nanolaminates, link between electrical and structural properties, J. Non-Cryst. Solids 303 (2002) 123-133.

[3] J. Meyer, P. Görrn, F. Bertram, S. Hamwi, T. Winkler, H.-H. Johannes, T. Weimann, P. Hinze, T. Riedl, W. Kowalsky, Al_2O_3/ZrO_2 nanolaminates as ultrahigh gas-diffusion barriers — A strategy for reliable encapsulation of organic electronics, Adv. Mater. 2009, 21, 1845-1849.

[4] C.R. Aita, Tailored ceramic film growth at low temperature by reactive sputter deposition, Critical Rev. Solid State Mater. Sci. 23 (1998) 205-274.

[5] Z. Tang, X. Zhu, H. Xu, Y. Xia, J. Yin, Z. Liu, A. Li, F. Yan, Impact of the interfaces in the charge trap layer on the storage characteristics of ZrO_2/Al_2O_3 nanolaminate-based charge trap flash memory cells, Mater. Lett. 92 (2013) 21-24.

[6] G. Balakrishnan, T.N. Sairam, V.R. Reddy, P. Kuppusami, J.I. Song, Microstructure and optical properties of Al_2O_3/ZrO_2 nanomultilayer thin films prepared by pulsed laser deposition, Mater. Chem. Phys. 140 (2013) 60-65.

[7] L. Zhong, F. Chen, S. A. Campbell, W. L. Gladfelter, Nanolaminates of zirconia and silica using atomic layer deposition, Chem. Mater. 16 (2004) 1098-1103.

[8] M. de Pauli, A. Malachias, H. Westfahl, Jr., J. Bettini, A. Ramirez, G. S. Huang, Y. F. Mei, O. G. Schmidt, Study of roughness evolution and layer stacking faults in short-period atomic layer deposited HfO_2/Al_2O_3 multilayers, J. Appl. Phys. 109 (2011) pp. 063524.

[9] O. Sneh, R. B. Clark-Phelps, A. R. Londergan, J. Winkler, T. E. Seidel, Thin film atomic layer deposition equipment for semiconductor processing, Thin Solid Films 402 (2002) 248-261.

[10] Y. S. Kim, S. J. Yun, Nanolaminated Al_2O_3–TiO_2 thin films grown by atomic layer deposition, J. Cryst. Growth 274 (2005) 585-593.

[11] S. Zaitsu, T. Jitsuno, M. Nakatsuka, T. Yamanaka, S. Motokoshi, Optical thin ®lms consisting of nanoscale laminated layers , Appl. Phys. Lett. Vol. 80 (2002) 2442-2444.

[12] D. R. G. Mitchell, D. J. Attard, K. S. Finnie, G. Triani, C.J. Barbé, C. Depagne, J.R. Bartlett, TEM and ellipsometry studies of nanolaminate oxide films prepared using atomic layer deposition, Appl. Surf. Sci. 243 (2005) 265-277.

[13] V. Mikhelashvili, G. Eisenstein, Composition, surface morphology and electrical characteristics of Al_2O_3–TiO_2 nanolaminates and AlTiO films on silicon, Thin Solid Films 515 (2006) 346-352.

[14] K. Kukli, J. Ihanus, M. Ritala, M. Leskelä, Properties of Ta2O5-based dielectric nanolaminates deposited by atomic layer epitaxy, J. Electrochem. Soc. 144 (1997) 300-306.

[15] A. Szeghalmi, S. Senz, M. Bretschneider, U. Gösele, M. Knez, All dielectric hard x-ray mirror by atomic layer deposition, Appl. Phys. Lett. 94 (2009) 133111-3.

[16] S.W. Smith, K.G. McAuliffe, J.F. Conley Jr., Atomic layer deposited high-k nanolaminate capacitors, Solid-State Electronics 54 (2010) 1076-1082.

[17] E. Härkönen, B. Diaz, b J. Światowska, V. Maurice, A. Seyeux, M. Vehkamäki, T. Sajavaara, M. Fenker, P. Marcus, M. Ritala, Corrosion protection of steel with oxide nanolaminates grown by atomic layer deposition, J. Electrochem. Soc. 158 (2011) C369-C378.

[18] H. Zhang, R. Solanki, Atomic layer deposition of high dielectric constant nanolaminates, J. Electrochem. Soc., 148 (2001) F63-F66.

[19] K. Kukli, J. Ihanus, M. Ritala, M. Leskelä, Tailoring the dielectric properties of HfO_2-Ta_2O_5 nanolaminates, Appl. Phys. Lett. 68 (1996) 3737-3739.

[20] H. Kim, P. C. McIntyre, K. C. Saraswat, Microstructural evolution of ZrO_2–HfO_2 nanolaminate structures grown by atomic layer deposition, J. Mater. Res.19 (2004) 643-650.

[21] A. Tamm, M. Heikkilä, M. Kemell, J. Kozlova, K. Kukli, V. Sammelselg, M. Ritala, M. Leskelä, Atomic layer deposition and characterization of zirconium oxide–erbium oxide nanolaminates, Thin Solid Films 519 (2010) 666-673.

[22] I. Jõgi, A. Tamm, K. Kukli, M. Kemell, J. Lu, T. Sajavaara, M. Ritala, M. Leskelä, J. Electrochem. Soc., Investigation of ZrO_2–Gd_2O_3 based high-k materials as capacitor dielectrics, 157 (2010) G202-G210.

[23] V. Sammelselg, A. Tarre, J. Lu, J. Aarik, A. Niilisk , T. Uustare, I. Netšipailo, R. Rammula, R. Pärna, A. Rosental, Structural characterization of TiO_2–Cr_2O_3 nanolaminates grown by atomic layer deposition, Surf. Coat. Tech. 204 (2010) 2015-2018.

[24] H. J. Cho, Y. D. Kim, D. S. Park, E. Lee, C. H. Park, J. S. Jang, K. B. Lee, H. W. Kim, Young Jong Ki, Il Keun Han, Yong Wook Song, New TIT Capacitor with $ZrO_2/Al_2O_3/ZrO_2$ dielectrics for 60nm and below DRAMs, Solid-State Electronics 51 (2007) 1529-1533.

[25] M. Ritala, M. Leskelä, L. Niinistö, T. Prohaska, G. Friedbacher, M. Grasserbauer, Surface roughness reduction in atomic layer epitaxy growth of titanium dioxide thin films, Thin Solid Films 249 (1994) 155-162.

[26] M. Laitinen, T. Sajavaara, M. Rossi, J. Julin, R. L. Puurunen, T. Suni, T. Ishida, H. Fujita, K. Arstila, B. Brijs, H. J. Whitlow, Depth profiling of Al_2O_3+TiO_2 nanolaminates by means of a time-of-flight energy spectrometer, Nucl. Instr. Methods Phys. Res. B 269 (2011) 3021-3024.

[27] K. Kukli, M. Kemell, M. C. Dimri, E. Puukilainen, A. Tamm, R. Stern, M. Ritala, M. Leskelä, Holmium titanium oxide thin films grown by atomic layer deposition, to be published.

[28] T. Suntola, Atomic layer epitaxy, Thin Solid Films 216 (1992) 84-89.

[29] J. Päiväsaari, M. Putkonen, L. Niinistö, A comparative study on lanthanide oxide thin films grown by atomic layer deposition, Thin Solid Films 472 (2005) 275-281.

[30] R. A. Waldo, Microbeam Analysis, San Francisco Press, San Francisco, CA,1988.

[40] H. Fujiwara, Spectroscopic Ellipsometry Principles and Applications, John Wiley & Sons Ltd, 2007.

[41] P. Eiamchai, P. Chindaudom, A. Pokaipisit, P. Limsuwan, A spectroscopic ellipsometry study of TiO_2 thin films prepared by ion-assisted electron-beam evaporation, Curr. Appl. Phys. 9 (2009) 707-712.

[42] M. Ritala, M. Leskelä, L. Niinistö, P. Haussalo, Titanium isopropoxide as a precursor in atomic layer epitaxy of titanium dioxide thin films, Chem. Mater. 5 (1993) 1174-1181.

[43] H. Siimon, J.Aarik, Thickness profiles of thin films caused by secondary reactions in flow-type atomic layer deposition reactors, J. Phys. D: Appl. Phys. 30 (1997) 1725-1728.

[44] T.-M. Pan, M.-D. Huang, C.-W. Lin, M.-H. Wu, Development of high-k $HoTiO_3$ sensing membrane for pH detection and glucose biosensing, Sens. Actuators B 144 (2010) 139-145.

[45] X. W. Dong, K. F. Wang, S. J. Luo, J. G. Wan, J.–M. Liu, Coexistence of magnetic and ferroelectric behaviors of pyrochlore $Ho_2Ti_2O_7$, J. Appl. Phys. 106 (2009) 104101.

[46] Y. Yang, D. S. Kim, R. Scholz, M. Knez, S. M. Lee, U. Gösele, M. Zacharias, Hierarchical three-dimensional ZnO and their shape-preserving transformation into hollow $ZnAl_2O_4$ nanostructures, Chem. Mater. 20 (2008) 3487-3494.

[47] M. P. Singh, K. D. Truong, P. Fournier, P. Rauwel, E. Rauwel, L. P. Carignan, D. Ménard, Anomalously large ferromagnetic Curie temperature of epitaxial Bi_2CoMnO_6 thin films, Appl. Phys. Lett. 92 (2008) 112505.

[48] R. I. Dass, J. B. Goodenough, Multiple magnetic phases of $La_2CoMnO_{6-\delta}$ ($0 \leq \delta \leq 0.05$) Phys. Rev. B 67 (2003) 014401.

[49] M. P. Singh, C. Grygiel, W. C. Sheets, Ph. Boullay, M. Hervieu, W. Prellier, B. Mercey, Ch. Simon, B. Raveau, Absence of long-range Ni/Mn ordering in ferromagnetic La_2NiMnO_6 thin films, Appl. Phys. Lett. 91 (2007) 012503.

CAPTIONS TO FIGURES:

Fig. **1**

Cross-sectional TEM (upper panel) and HRTEM (lower panel) images of a Ho_2O_3-TiO_2 nanolaminate in the as-deposited state. The constituent layer materials are indicated by labels.

Fig. **2**

Cross-sectional EDX composition profiling of the Ho_2O_3-TiO_2 nanolaminate in the as-deposited state. The elements detected are indicated by labels. Due to the higher O concentration in TiO_2 compared to that in Ho_2O_3, the O profile is following the Ti profile rather than Ho (color online).

Fig. **3**

Spectroscopic ellipsometry results of the Ho_2O_3-TiO_2 nanolaminate in the as-deposited state. Upper panels depict the Δ and ψ curves measured together with the fitting results. The 3rd panel from the top represents the multilayer schematics with the thicknesses and refractive indexes giving the best fit with measured spectra. The bottom panel demonstrates total multilayer thickness map over a Si(100) substrate with an area of 5 × 5 cm × cm.

Fig. **4**

X-ray diffraction patterns from the Ho_2O_3-TiO_2 nanolaminate in the as-deposited state, and after annealing at 800 and 1000 °C in N_2 for 30 min. Miller indexes assigned after crystallization to the pyrochlore phase $Ho_2Ti_2O_7$ are indicated.

Fig. **5**

HRTEM images in two different scales (top and middle panels) and compositional EDX map (bottom panel) from the Ho_2O_3-TiO_2 nanolaminate annealed at 1000 °C in N_2 for 30 min. (color online)

Fig. **6**

Atomic force microscopy height (left column) and phase (right column) images of the Ho_2O_3-TiO_2 nanolaminate in the as-deposited state (upper row) and after annealing at 800 °C in N_2 for 30 min (lower row).

Fig. **7**

X-ray reflectivity patterns measured from Ho_2O_3-TiO_2 nanolaminate at different annealing temperatures in three-dimensional (a) and conventional (b) mode.

Fig. **8**

Magnetization vs. measurement temperature (upper panel) and magnetic moment vs. external magnetic field curves (lower panel) for the Ho_2O_3-TiO_2 nanolaminate in the as-deposited state. The measurement field for ***M***-T and temperatures for ***M***-***H*** curves are indicated by labels.

Fig. **9**

Magnetization vs. measurement temperature (the 1st and 2nd panels from top) and magnetic moment vs. external magnetic field (***M***-***H***) curves (the 3rd and 4th panels) for the Ho_2O_3-TiO_2 nanolaminate after annealing at 800 °C in N_2 for 30 min. The measurement temperatures for ***M***-***H*** curves are indicated by labels.

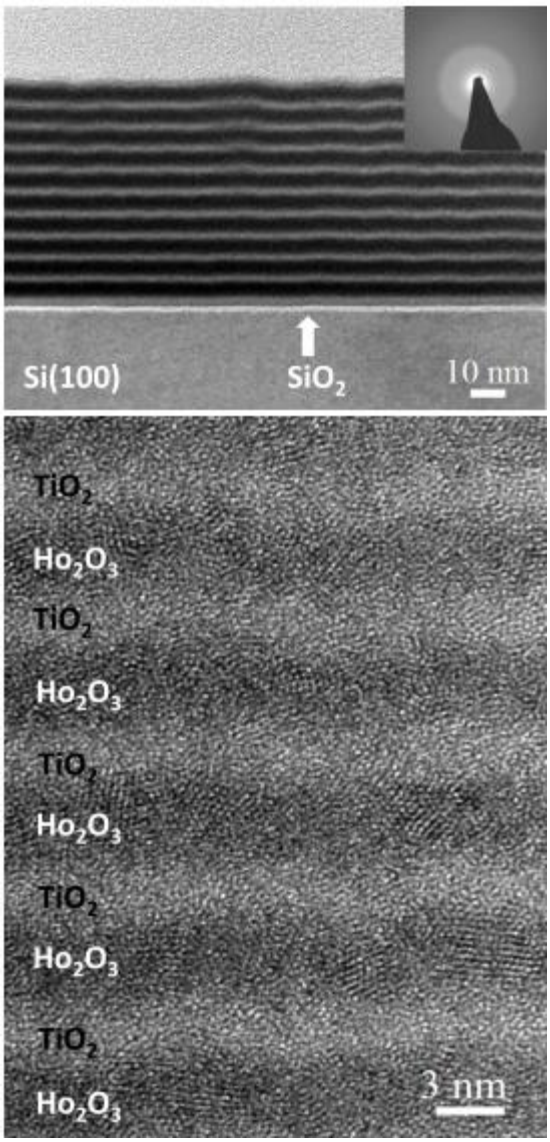

Fig.1 Kukli et al.

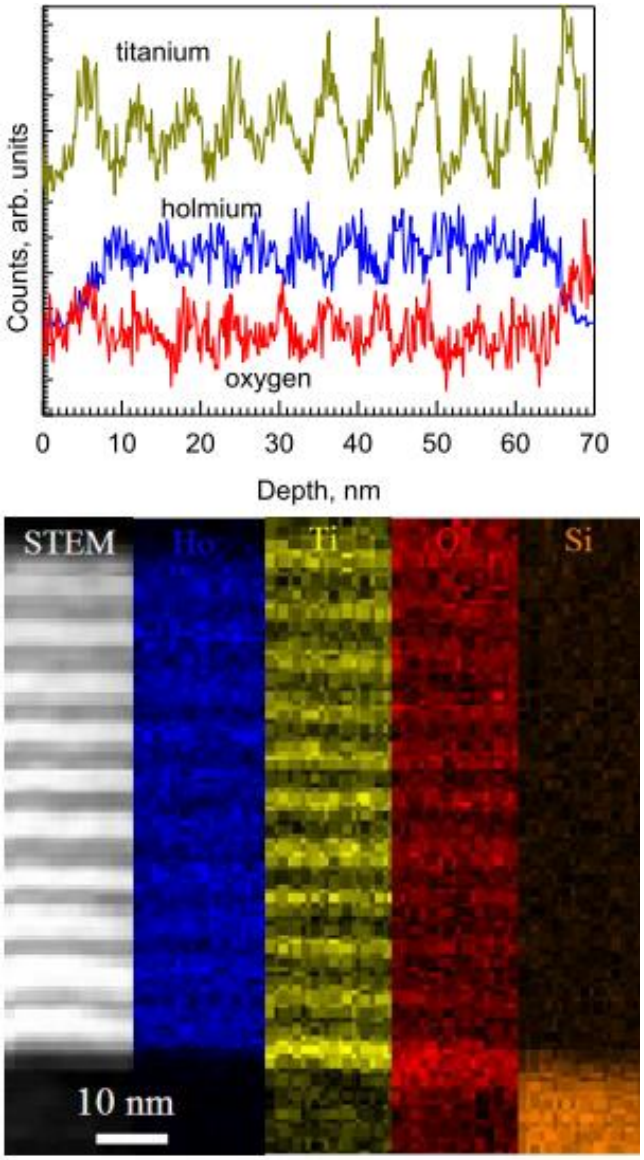

Fig. 2 Kukli et al.

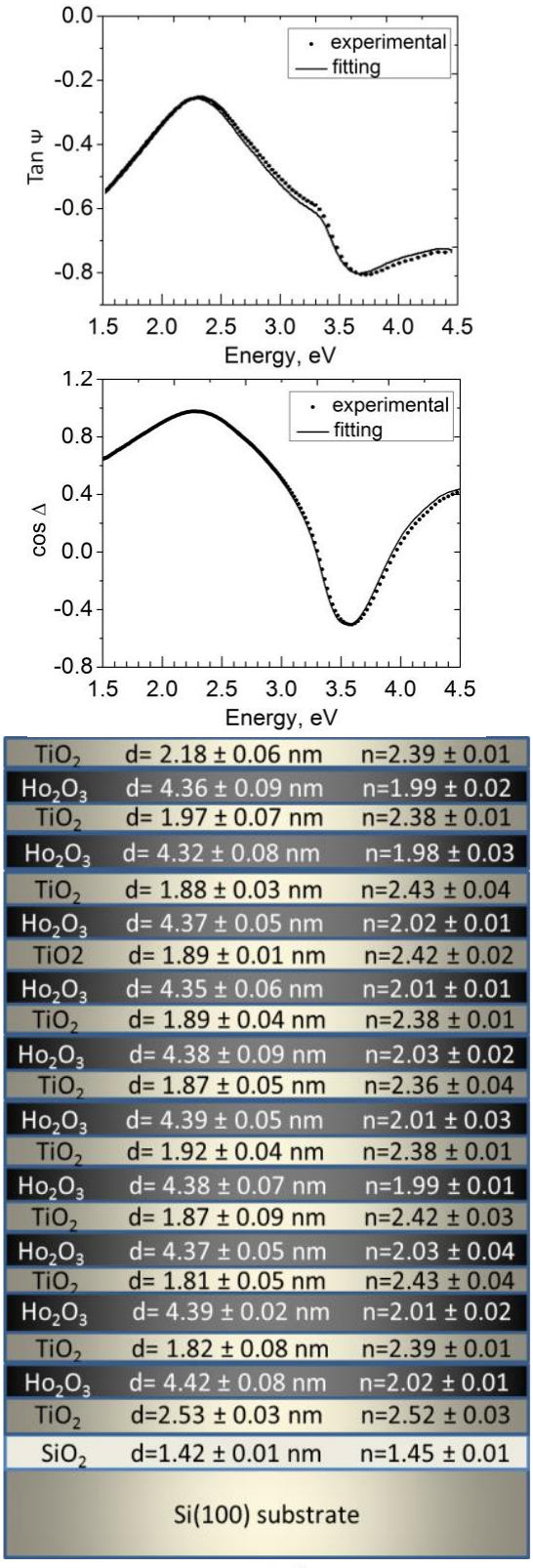

Fig. **3** Kukli *et al*.

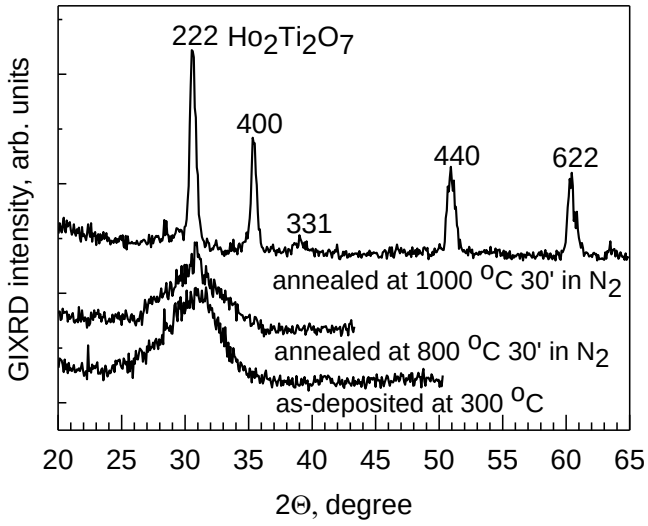

Fig. 4 Kukli et al.

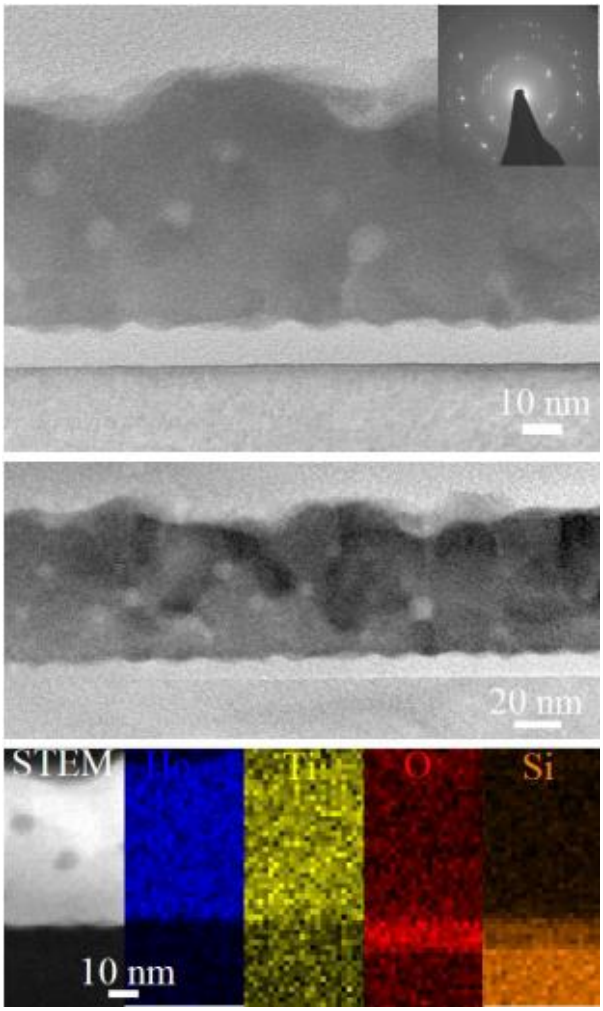

Fig. 5 Kukli et al.

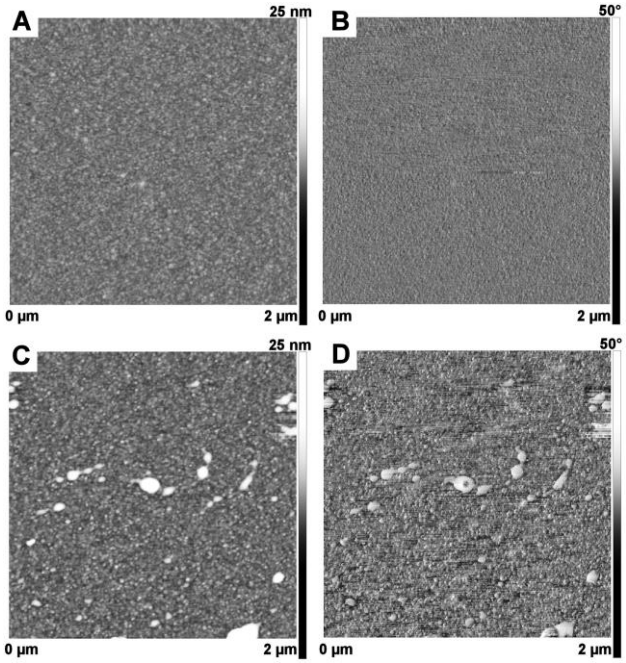

Fig. 6 Kukli et al.

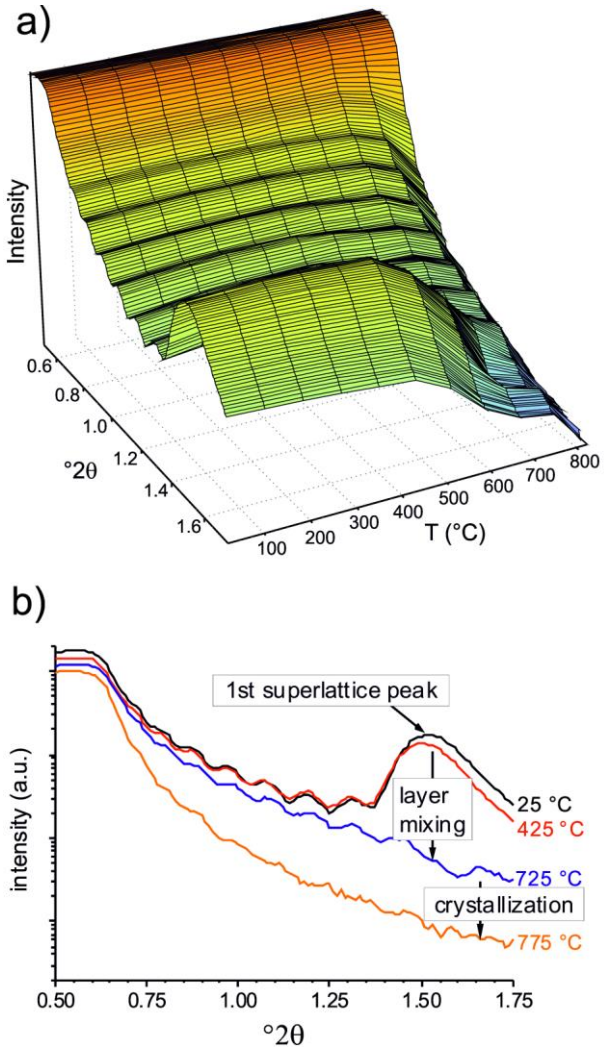

Fig. **7** Kukli et al.

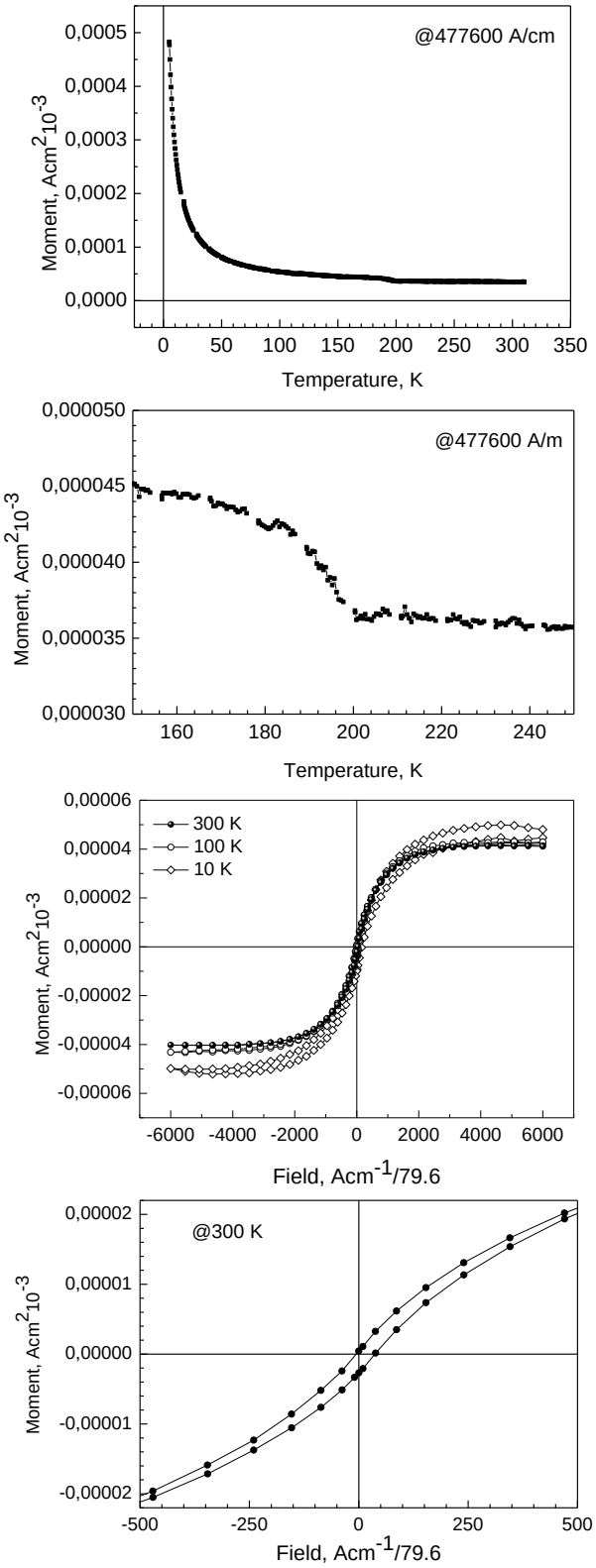

Fig. 8 Kukli et al.